further supported that IQGAP1 is positively involved in the process of hepatotumorigenesis. This is the first report to document the stepwise increase of IQGAP1 mRNA and protein expression in a rat model of naturally occurring oxidative stress-induced hepatotumorigenesis. In *Iqgap2*$^{-/-}$ mice, HCC develops in an IQGAP1-dependent manner, while overexpression of IQGAP1 is associated with acquired β-catenin mutations, and dephosphorylated (active) β-catenin accumulates specifically in HCC livers but not in liver tissue from younger wild-type or *Iqgap2*$^{-/-}$ mice without HCC (37).

Vimentin is a cytoplasmic intermediate filament protein synthesized in cells of mesenchymal origin. It is therefore usually expressed in mesenchymal but not epithelial cells, and high vimentin expression in tumor epithelial cells has been correlated with tumorigenic potential, marked by the growth, invasive and migratory ability of cancer cells (38,39). Vimentin knockdown by RNA interference reduces cancer cell activities, resulting in greatly decreased tumorigenic potential (39,40). Reversal of the mesenchymal phenotype by inhibition of vimentin expression restores epithelial characteristics to cells *in vitro* (keratin gene expression) and smaller more differentiated tumors *in vivo* (39). Vimentin expression is also known as a sign of epithelial-to-mesenchymal transition, originally defined as the formation of mesenchymal cells from epithelia during the embryonic stages of development. In this process, the progression of tumors with strong malignant potential requires the epithelial phenotype to be lost along with junctional proteins such as E-cadherin and polarizing of the cells. Meanwhile, the cell acquires a more mesenchymal phenotype with reduced cell–cell adhesion, unpolarized spindle-shaped morphology (fibroblasts and fibroblast-like cells), enhanced cell motility and the presence of mesenchymal cellular markers such as vimentin (41,42).

In fact, advanced liver tumors in LEC rats spread over the liver in a scirrhous growth pattern and sometimes metastasize to lymph nodes. It is noteworthy that the expression levels of vimentin mRNA and protein increased in a stepwise manner during tumorigenesis in this study. Similar to IQGAP1, vimentin was latently upregulated before the development of liver tumors. It also increases in CCl_4-induced cirrhotic mouse livers, whereby hepatocytes derived from such livers and maintained *in vitro* exhibit high expression of vimentin and low expression E-cadherin, with the morphological characteristics of epithelial-to-mesenchymal transition (43). Prolonged exposure of mouse hepatocytes to transforming growth factor-β increases vimentin expression, suggesting that hepatocytes may have fibrogenic potential (44).

The text-mining software used in this study aimed to utilize more comprehensive and recent gene–gene interaction data (http://www.nalapro.com) than manual curation pathway databases, such as Ingenuity Pathway Analysis (45) and MetaCore (46). Moreover, the software provides interaction data with directional information among genes by using natural language processing/text-mining technology, unlike machine curation pathway databases, such as PubGene (47) and BiblioSphere (48), which use a different text-mining algorithm. Bioinformatics, such as integration of additional biological interactive data, is needed to uncover the molecular mechanisms underlying hepatotumorigenesis because the inherently complex and multivariate relations in gene regulatory network lead to difficulties in data interpretation.

In conclusion, IQGAP1 and vimentin were stepwise upregulated in an animal model with naturally occurring and oxidative stress-induced hepatotumorigenesis, implicating both as major molecules initiated and promoted by persistent oxidative stress, as key regulator genes involved in the multistep process of liver tumorigenesis and as targets for the development of novel gene therapies.

Supplementary material

Supplementary Tables 1 and 2 and Figures 1 and 2 can be found at http://carcin.oxfordjournals.org/

Funding

Grant-in-Aid for Scientific Research from the Ministry of Education, Culture, Sports, Science and Technology (Japan) (90322643 to A.T.).

Acknowledgements

We thank Ms Noriko Hashimoto (National Research Institute for Child Health and Development), Ms Mamiko Ohwada, Ms Rie Agata, Ms Yoko Yumoto and Mr Yasuo Mabashi (Jikei University School of Medicine) for the skillful technical assistance.

Conflict of Interest Statement: None declared.

References

1. Obama,K. *et al.* (2005) Genome-wide analysis of gene expression in human intrahepatic cholangiocarcinoma. *Hepatology*, **41**, 1339–1348.
2. Hass,H.G. *et al.* (2008) Identification of osteopontin as the most consistently over-expressed gene in intrahepatic cholangiocarcinoma: detection by oligonucleotide microarray and real-time PCR analysis. *World J. Gastroenterol.*, **14**, 2501–2510.
3. Iizuka,N. *et al.* (2008) Translational microarray systems for outcome prediction of hepatocellular carcinoma. *Cancer Sci.*, **99**, 659–665.
4. Farazi,P.A. *et al.* (2006) Hepatocellular carcinoma pathogenesis: from genes to environment. *Nat. Rev. Cancer*, **6**, 674–687.
5. Blechacz,B. *et al.* (2008) Cholangiocarcinoma: advances in pathogenesis, diagnosis, and treatment. *Hepatology*, **48**, 308–321.
6. Hammill,C.W. *et al.* (2008) Intrahepatic cholangiocarcinoma: a malignancy of increasing importance. *J. Am. Coll. Surg.*, **207**, 594–603.
7. Rosenthal,P. (2008) Hepatocarcinoma in viral and metabolic liver disease. *J. Pediatr. Gastroenterol. Nutr.*, **46**, 370–375.
8. Okabe,H. *et al.* (2001) Genome-wide analysis of gene expression in human hepatocellular carcinomas using cDNA microarray: identification of genes involved in viral carcinogenesis and tumor progression. *Cancer Res.*, **61**, 2129–2137.
9. Iizuka,N. *et al.* (2002) Comparison of gene expression profiles between hepatitis B virus- and hepatitis C virus-infected hepatocellular carcinoma by oligonucleotide microarray data on the basis of a supervised learning method. *Cancer Res.*, **62**, 3939–3944.
10. Schwarz,K.B. (1996) Oxidative stress during viral infection: a review. *Free Radic. Biol. Med.*, **21**, 641–649.
11. Shacter,E. *et al.* (2002) Chronic inflammation and cancer. *Oncology*, **16**, 217–226, 229; (discussion 230–232).
12. Marrogi,A.J. *et al.* (2001) Oxidative stress and p53 mutations in the carcinogenesis of iron overload-associated hepatocellular carcinoma. *J. Natl Cancer Inst.*, **93**, 1652–1655.
13. Kurz,D.J. *et al.* (2004) Chronic oxidative stress compromises telomere integrity and accelerates the onset of senescence in human endothelial cells. *J. Cell Sci.*, **117**, 2417–2426.
14. Wu,J. *et al.* (1994) The LEC rat has a deletion in the copper transporting ATPase gene homologous to the Wilson disease gene. *Nat. Genet.*, **7**, 541–545.
15. Masuda,R. *et al.* (1988) High susceptibility to hepatocellular carcinoma development in LEC rats with hereditary hepatitis. *Jpn. J. Cancer Res.*, **79**, 828–835.
16. Sone,K. *et al.* (1996) Inhibition of hereditary hepatitis and liver tumor development in Long-Evans cinnamon rats by the copper-chelating agent trientine dihydrochloride. *Hepatology*, **23**, 764–770.
17. Meerson,N.R. *et al.* (1998) Identification of B10, an alkaline phosphodiesterase of the apical plasma membrane of hepatocytes and biliary cells, in rat serum: increased levels following bile duct ligation and during the development of cholangiocarcinoma. *Hepatology*, **27**, 563–568.
18. Hensley,K. *et al.* (2000) Reactive oxygen species, cell signaling, and cell injury. *Free Radic. Biol. Med.*, **28**, 1456–1462.
19. Stohs,S.J. *et al.* (1995) Oxidative mechanisms in the toxicity of metal ions. *Free Radic. Biol. Med.*, **18**, 321–336.
20. Kushida,T. *et al.* (2009) *Collection of disease networks by hybrid curation method and the application for pathway analysis.* Proceedings of 2nd International Workshop on Intelligent Informatics in Biology and Medicine, 16–19 March 2009, Fukuoka, Japan, 800–806.
21. Shannon,P. *et al.* (2003) Cytoscape: a software environment for integrated models of biomolecular interaction networks. *Genome Res.*, **13**, 2498–2504.
22. Briggs,M.W. *et al.* (2003) IQGAP proteins are integral components of cytoskeletal regulation. *EMBO Rep.*, **4**, 571–574.
23. Mateer,S.C. (2003) IQGAPs: integrators of the cytoskeleton, cell adhesion machinery, and signaling networks. *Cell Motil. Cytoskeleton*, **55**, 147–155.
24. Noritake,J. *et al.* (2005) IQGAP1: a key regulator of adhesion and migration. *J. Cell Sci.*, **118**, 2085–2092.

25. Brown,M.D. (2006) IQGAP1 in cellular signaling: bridging the GAP. *Trends Cell Biol.*, **16**, 242–249.
26. Kuroda,S. *et al.* (1998) Role of IQGAP1, a target of the small GTPases Cdc42 and Rac1, in regulation of E-cadherin- mediated cell-cell adhesion. *Science*, **281**, 832–835.
27. Jadeski,L. *et al.* (2008) IQGAP1 stimulates proliferation and enhances tumorigenesis of human breast epithelial cells. *J. Biol. Chem.*, **283**, 1008–1017.
28. Walch,A. *et al.* (2008) Combined analysis of Rac1, IQGAP1, Tiam1 and E-cadherin expression in gastric cancer. *Mod. Pathol.*, **21**, 544–552.
29. Yamaoka-Tojo,M. *et al.* (2004) IQGAP1, a novel vascular endothelial growth factor receptor binding protein, is involved in reactive oxygen species—dependent endothelial migration and proliferation. *Circ. Res.*, **95**, 276–283.
30. Meyer,R.D. *et al.* (2008) IQGAP1-dependent signaling pathway regulates endothelial cell proliferation and angiogenesis. *PLoS ONE*, **3**, e3848; (1–11).
31. Sugimoto,N. *et al.* (2001) IQGAP1, a negative regulator of cell-cell adhesion, is upregulated by gene amplification at 15q26 in gastric cancer cell lines HSC39 and 40A. *J. Hum. Genet.*, **46**, 21–25.
32. Takemoto,H. *et al.* (2001) Localization of IQGAP1 is inversely correlated with intercellular adhesion mediated by e-cadherin in gastric cancers. *Int. J. Cancer*, **91**, 783–788.
33. Sun,W. *et al.* (2004) Identification of differentially expressed genes in human lung squamous cell carcinoma using suppression subtractive hybridization. *Cancer Lett.*, **212**, 83–93.
34. Nabeshima,K. *et al.* (2002) Immunohistochemical analysis of IQGAP1 expression in human colorectal carcinomas: its overexpression in carcinomas and association with invasion fronts. *Cancer Lett.*, **176**, 101–109.
35. Dong,P. *et al.* (2006) Overexpression and diffuse expression pattern of IQGAP1 at invasion fronts are independent prognostic parameters in ovarian carcinomas. *Cancer Lett.*, **243**, 120–127.
36. Balenci,L. *et al.* (2006) IQGAP1 protein specifies amplifying cancer cells in glioblastoma multiforme. *Cancer Res.*, **66**, 9074–9082.
37. Schmidt,V.A. *et al.* (2008) Development of hepatocellular carcinoma in Iqgap2-deficient mice is IQGAP1 dependent. *Mol. Cell. Biol.*, **28**, 1489–1502.
38. Bindels,S. *et al.* (2006) Regulation of vimentin by SIP1 in human epithelial breast tumor cells. *Oncogene*, **25**, 4975–4985.
39. Paccione,R.J. *et al.* (2008) Keratin down-regulation in vimentin-positive cancer cells is reversible by vimentin RNA interference, which inhibits growth and motility. *Mol. Cancer Ther.*, **7**, 2894–2903.
40. McInroy,L. *et al.* (2007) Down-regulation of vimentin expression inhibits carcinoma cell migration and adhesion. *Biochem. Biophys. Res. Commun.*, **360**, 109–114.
41. Thiery,J.P. (2002) Epithelial-mesenchymal transitions in tumour progression. *Nat. Rev. Cancer*, **2**, 442–454.
42. Huber,M.A. *et al.* (2005) Molecular requirements for epithelial-mesenchymal transition during tumor progression. *Curr. Opin. Cell Biol.*, **17**, 548–558.
43. Nitta,T. *et al.* (2008) Murine cirrhosis induces hepatocyte epithelial mesenchymal transition and alterations in survival signaling pathways. *Hepatology*, **48**, 909–919.
44. Kaimori,A. *et al.* (2007) Transforming growth factor-beta1 induces an epithelial-to-mesenchymal transition state in mouse hepatocytes *in vitro*. *J. Biol. Chem.*, **282**, 22089–22101.
45. Calvano,S.E. *et al.* (2005) A network-based analysis of systemic inflammation in humans. *Nature*, **437**, 1032–1037.
46. Ekins,S. *et al.* (2007) Pathway mapping tools for analysis of high content data. *Methods Mol. Biol.*, **356**, 319–350.
47. Jenssen,T.K. *et al.* (2001) A literature network of human genes for high-throughput analysis of gene expression. *Nat. Genet.*, **28**, 21–28.
48. Scherf,M. *et al.* (2005) The next generation of literature analysis: integration of genomic analysis into text mining. *Brief. Bioinform.*, **6**, 287–297.

Received April 23, 2009; revised December 7, 2009; accepted December 9, 2009

World Journal of Radiology

Online Submissions: http://www.wjgnet.com/1949-8470office
wjr@wjgnet.com
doi:10.4329/wjr.v2.i6.215

World J Radiol 2010 June 28; 2(6): 215-223
ISSN 1949-8470 (online)

TOPIC HIGHLIGHT

Hui-Xiong Xu, MD, PhD, *Series Editor*

Computer-aided diagnosis for contrast-enhanced ultrasound in the liver

Katsutoshi Sugimoto, Junji Shiraishi, Fuminori Moriyasu, Kunio Doi

Katsutoshi Sugimoto, Junji Shiraishi, Kunio Doi, Kurt Rossmann Laboratories for Radiologic Imaging Research, Department of Radiology, The University of Chicago, Chicago, IL 60637, United States
Katsutoshi Sugimoto, Fuminori Moriyasu, Department of Gastroenterology and Hepatology, Tokyo Medical University, Tokyo 160-0023, Japan
Junji Shiraishi, School of Health Sciences, Kumamoto University, Kumamoto 862-0976, Japan
Author contributions: All authors analyzed and interpreted the data; Sugimoto K drafted the manuscript; Sugimoto K and Doi K researched the literature; Shiraishi J and Doi K edited the manuscript.
Correspondence to: Katsutoshi Sugimoto, MD, Department of Gastroenterology and Hepatology, Tokyo Medical University, Japan 6-7-1 Nishishinjuku, Shinjuku-ku, Tokyo 160-0023, Japan. sugimoto@tokyo-med.ac.jp
Telephone: +81-3-33426111 Fax: +81-3-53816654
Received: February 21, 2010 Revised: May 6, 2010
Accepted: May 13, 2010
Published online: June 28, 2010

Abstract

Computer-aided diagnosis (CAD) has become one of the major research subjects in medical imaging and diagnostic radiology. The basic concept of CAD is to provide computer output as a second opinion to assist radiologists' image interpretations by improving the accuracy and consistency of radiologic diagnosis and also by reducing the image-reading time. To date, research on CAD in ultrasound (US)-based diagnosis has been carried out mostly for breast lesions and has been limited in the fields of gastroenterology and hepatology, with most studies being conducted using B-mode US images. Two CAD schemes with contrast-enhanced US (CEUS) that are used in classifying focal liver lesions (FLLs) as liver metastasis, hemangioma, or three histologically differentiated types of hepatocellular carcinoma (HCC) are introduced in this article: one is based on physicians' subjective pattern classifications (subjective analysis) and the other is a computerized scheme for classification of FLLs (quantitative analysis). Classification accuracies for FLLs for each CAD scheme were 84.8% and 88.5% for metastasis, 93.3% and 93.8% for hemangioma, and 98.6% and 86.9% for all HCCs, respectively. In addition, the classification accuracies for histologic differentiation of HCCs were 65.2% and 79.2% for well-differentiated HCCs, 41.7% and 50.0% for moderately differentiated HCCs, and 80.0% and 77.8% for poorly differentiated HCCs, respectively. There are a number of issues concerning the clinical application of CAD for CEUS, however, it is likely that CAD for CEUS of the liver will make great progress in the future.

Key words: Computer-aided diagnosis; Focal liver lesion; Ultrasonography; Contrast agent; Micro-flow imaging

Peer reviewer: Juan Xu, PhD, University of Pittsburgh School of Medicine, UPMC Eye Center, 203 Lothrop St EEI- 835, Pittsburgh, PA 15213, United States

Sugimoto K, Shiraishi J, Moriyasu F, Doi K. Computer-aided diagnosis for contrast-enhanced ultrasound in the liver. *World J Radiol* 2010; 2(6): 215-223 Available from: URL: http://www.wjgnet.com/1949-8470/full/v2/i6/215.htm DOI: http://dx.doi.org/10.4329/wjr.v2.i6.215

INTRODUCTION

Ultrasound (US) is an easy-to-use and minimally invasive imaging modality that is useful for detection and qualitative diagnosis of focal liver lesions (FLLs). In addition, the detection and qualitative diagnosis of FLLs have been markedly improved by the development of US contrast agents consisting of microbubbles[1-5] and by harmonic imaging that can visualize nonlinear scattering of microbubbles[6-12].

It is well known that a major problem with US examinations is their operator-dependent nature, as compared with computed tomography (CT) and magnetic resonance (MR) imaging[13]. It is therefore necessary to reduce the operator-dependent limitations of US examinations. Computer-aided diagnosis (CAD) may be an approach that overcomes this problem.

To date, research on CAD in US-based diagnosis has been carried out mostly on breast lesions[14-19] and has been limited in the fields of gastroenterology and hepatology. In this article, we introduce CAD aimed at differential diagnosis of FLLs by use of contrast-enhanced US (CEUS), in addition to reviewing CAD on US in liver research.

WHAT IS CAD?

Recently, CAD has become a major research subject in medical imaging and diagnostic radiology[20-24]. Many different types of CAD schemes are being developed for the detection and/or characterization of lesions in various tissues using medical imaging, including conventional projection radiography, CT, MR imaging, and US. CAD research is being carried out on detecting lesions in breast, chest, colon, brain, liver and kidney, as well as the vascular and skeletal systems.

CAD is defined as a diagnosis made by a physician who takes into account the computer output based on quantitative analysis of radiologic images. This definition is clearly distinct from automated computerized diagnosis[25-27], which was attempted in the 1960s and 1970s and included replacing radiologists by computers. Subsequently, Doi *et al*[20-22] began their investigations on CAD at the University of Chicago in the 1980s with a clear goal of assisting radiologists with computerized information. The goal of CAD research is to improve the quality and productivity of radiologists' tasks by improving the accuracy and consistency of radiologic diagnoses and also by reducing the image-reading time.

CURRENT STATUS OF RESEARCH ON CAD BASED ON US OF THE LIVER

To date, CAD based on US of the liver has been frequently used in diffuse liver disease for quantifying the degree of liver fibrosis and fat deposition[28-30]. In addition, CAD for FLLs has been reported[31-34]; however, the number of such reports is small compared with the reports on CAD for diffuse liver disease. This is somewhat surprising because computers are, in general, superior to humans in quantitative measurements and in differential diagnosis, but inferior in lesion detection because of a large number of false positives. However, CAD has been used for quantitative evaluation of liver volume for support treatment, which included liver resection and radiofrequency ablation therapy applied to hepatocellular carcinoma (HCC) by application of volume measurements in 3D-US images[35,36]. All such applications have been developed based on B-mode US images.

Second-generation US contrast agents have been developed recently. Definity (Lantheus Inc., MA, USA) and SonoVue (Bracco, Milan, Italy) became available commercially in Canada and Europe, respectively, in 2001, whereas SonoVue became available in China in 2006, followed by Sonazoid (Daiichi Sankyo, Tokyo, Japan) in Japan in 2007 and SonoVue in Korea in 2008. Their utility for the diagnosis of FLLs has been reported[1-5]. In parallel, CAD with CEUS images for differentiating FLLs has been reported[33,34]. In these studies, FLLs were diagnosed by analysis of relatively simple blood flow parameters obtained from measurements of the time-intensity curve (TIC), which reflects tumor hemodynamics. Thus, research on CAD with CEUS images of the liver has just begun worldwide. In the next section, we introduce two different types of CAD schemes aimed at the differential diagnosis of FLLs, which were developed in collaboration with colleagues at the University of Chicago as examples of CAD[31,32].

SUBJECTIVE CLASSIFICATION OF FLLs USING PHYSICIANS' SUBJECTIVE PATTERN CLASSIFICATIONS (SUBJECTIVE ANALYSIS)

In this study, a total of 137 nodules in 137 cases were used for the development of CAD; specifically, there were 74 HCCs [23 well-differentiated (w-HCC), 36 moderately differentiated (m-HCC) and 15 poorly differentiated (p-HCC)], 33 liver metastases and 30 liver hemangiomas. HCC and liver metastasis were diagnosed based on histology after liver resection or liver biopsy in all cases. Liver hemangioma was diagnosed by contrast-enhanced CT and/or MR imaging. The US equipment used in this study was an SSA-790A (Aplio™XG; Toshiba Medical Systems Co., Otawara, Japan). The imaging mode was wideband harmonic imaging (commercially called Pulse subtraction) with transmission and reception frequencies of 3.75 MHz and 7.5 MHz, respectively. The contrast agent used was Sonazoid, which consists of perflubutane-based microbubbles surrounded by phospholipids with a median diameter of 2-3 μm.

From the baseline US features of an FLL, three experienced physicians were requested to classify the echogenic patterns of the FLL into one of the following eight patterns: (1) hyperechoic; (2) hypoechoic; (3) anechoic; (4) thin hypoechoic rim; (5) thick hypoechoic rim (bull's eye); (6) hyperechoic rim; (7) mosaic; and (8) others (Figure 1A). These patterns were proposed by Itai *et al*[37] for describing the characteristics of FLLs from baseline US.

After rating the echogenic patterns of FLLs from baseline US, the physicians were asked to classify the contrast-enhancement patterns of FLLs into one of the following eight patterns: (1) absent; (2) dotted; (3) peripheral rimlike; (4) peripheral nodular; (5) central with spoke wheel-shape; (6) diffuse heterogeneous; (7) diffuse homogeneous; and (8) others (Figure 1B). These patterns were proposed by

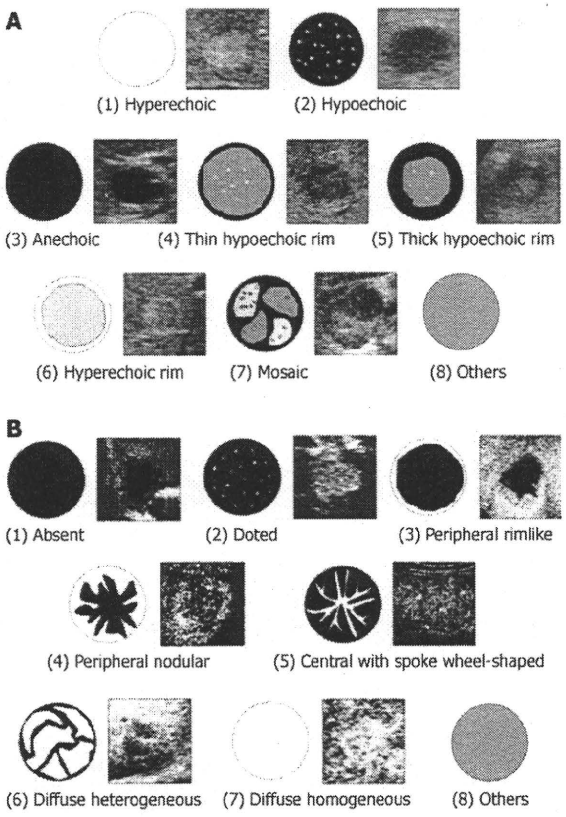

Figure 1 Hepatic tumors. A: Illustration of morphologic patterns of hepatic tumors in the B-mode ultrasonography; B: Illustration of enhancement patterns of hepatic tumors in the arterial phase.

Quaia *et al*[38]. The physicians were not asked to provide a diagnosis in this study.

For analysis of the subjective ratings obtained by the three physicians, we created a matrix of 137 FLLs and 16 patterns, which indicated the total number of physicians who rated lesions in each pattern.

To classify the five types of FLLs (i.e. w-HCCs, m-HCCs, p-HCCs, metastases and hemangiomas) in this CAD scheme, we employed four artificial neural networks (ANNs), as shown in Figure 2. ANNs are mathematical models based on biologic neural networks, which consist of an interconnected group of artificial neurons that can process information by using a connectionist approach to computation. The order of the four decisions (labeled D1-D4) in each ANN was determined by considering the diagnostic difficulty, which was based on the physicians' knowledge levels. The four decisions used in this study were the following: (1) D1: Is this lesion an HCC (yes) or other (no)? (2) D2: Is this lesion a hemangioma (yes) or metastasis (no)? (3)D3: Is this lesion a p-HCC (yes) or other HCC (no)? and (4) D4: Is this lesion a w-HCC (yes) or a m-HCC (no)?

All decisions were determined using each of the ANNs with a two-alternative choice method. In the learning and testing process of the ANNs, a leave-one-out test was employed in individual ANNs. In this method, one

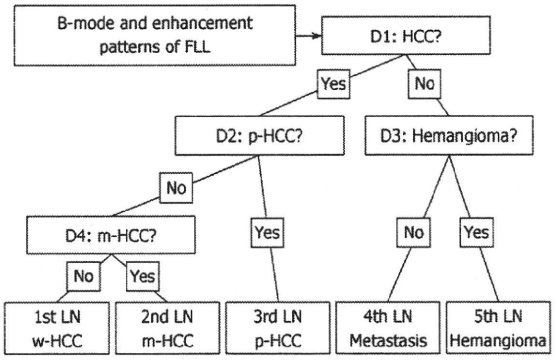

Figure 2 Illustration of the decision tree model used in this study. Four decision nodes in which alternative choice was determined by all five FLLs, leading to a final diagnostic decision for five liver lesions. D: Decision node; FLL: Focal liver lesion; HCC: Hepatocellular carcinoma; LN: Leaf node; m-HCC: Moderately differentiated HCC; p-HCC: Poorly differentiated HCC; w-HCC: Well-differentiated HCC.

case is left out for a test, and the ANN is trained to learn using the remaining cases. The one case that was left out is used for testing the trained ANN. The same procedure was then repeated until all cases were tested.

In the four ANNs, we did not use one of the subjective classifications (i.e. others), because we assumed that uncertain data might have a detrimental effect on the training of the ANNs. Thus, we used 14 input units corresponding to seven patterns of subjective classification data in the matrix as described previously.

The correct classification of the CAD scheme for the five types of FLLs was determined when the final outcome from the four ANNs agreed with the "gold standard". The classification accuracies for each type of FLL and also for all 137 FLLs were determined with the percentages of correctly classified cases among the total number of cases.

Table 1 shows the performance of the computerized scheme for the classification of the five types of FLLs. The classification accuracies for the 137 FLLs were 84.8% for metastasis, 93.3% for hemangioma, 65.2% for w-HCC, 41.7% for m-HCC, and 80.0% for p-HCC. When the classification was conducted only for three types of FLLs (i.e. HCCs, metastasis, and hemangioma), the classification accuracy for all HCCs was 98.6%, as shown in Table 2. The average classification accuracies for the three and five types of FLLs were 94.2% and 71.5%, respectively.

COMPUTERIZED SCHEME FOR CLASSIFICATION OF FLLs

Micro-flow imaging with contrast-enhanced ultrasonography

Micro-flow imaging (MFI; Toshiba Medical Systems Co., Otawara, Japan) is a novel image-processing technique that is accompanied by high-mechanical-index (MI > 1.0) disruptive flash frames and the maximum intensity projection (MIP) technique[32,39]. MIP processing is initi-

Table 1 Performance of CAD scheme for classification in five categories using physicians' pattern classification *n* (%)

Lesion	*n*	Classification with CAD				
		HCC			Metastasis	Hemangioma
		w-HCC	m-HCC	p-HCC		
HCC	74					
w-HCC	23	15 (65.2)	4 (17.4)	4 (17.4)	0 (0.0)	0 (0.0)
m-HCC	36	16 (44.4)	15 (41.7)	5 (13.9)	0 (0.0)	1 (2.7)
p-HCC	15	1 (6.7)	1 (6.7)	12 (80.0)	1 (6.7)	0 (0.0)
Metastasis	33	1 (3.0)	0 (0.0)	1 (3.0)	28 (84.8)	3 (9.1)
Hemangioma	30	0 (0.0)	0 (0.0)	1 (3.3)	1 (3.3)	28 (93.3)

Overall diagnostic accuracy: 98/137 (71.5%). CAD performance was evaluated by a leave-one-case-out methods. Reproduced, with modification, form Sugimoto *et al*[31], *Acad Radiol* 2009; 16: 401-411. CAD: Computer-aided diagnosis; HCC: Hepatocellular carcinoma; w-HCC: Well-differentiated HCC; m-HCC: Moderately differentiated HCC; p-HCC: Poorly differentiated HCC.

Table 2 Performance of CAD scheme for classification in three categories using physicians' subjective pattern classification *n* (%)

Lesion	*n*	Classification with CAD		
		HCC	Metastasis	Hemangioma
HCC	74	73 (98.6)	1 (1.4)	0 (0.0)
Metastasis	33	2 (6.1)	28 (84.8)	3 (9.1)
Hemangioma	30	1 (3.3)	1 (3.3)	28 (93.3)

Overall diagnostic accuracy: 129/137 (94.2%). CAD performance was evaluated by a leave-one-case out method. Reproduced, with modification, form Sugimoto *et al*[31], *Acad Radiol* 2009; 16: 401-411.

ated after a sonographic flash frame disrupts bubbles in the field of view. Using this technique, we could obtain information about the microbubble pathway between frames and observe exquisite detail of lesional vessels, with the potential to show both their morphology and their direction of filling[32,39,40].

To date, some investigators[39,41] have reported that the intratumoral vasculature of HCCs was clearly visualized using this technique and pattern classification was possible; these results suggested the possibility of differential diagnosis of the degree of HCCs[39,41]. CEUS with MFI could be useful for diagnosis of HCCs, and other FLLs, because MFI can depict the minute intratumoral vasculature of the tumor better than harmonic imaging. In this study, we therefore used various kinds of image features that can be derived from MFI findings as input data for the CAD.

Image database

A total of 103 nodules in 97 cases were used for the development of CAD. In more detail, there were 61 HCCs (24 w-HCC, 28 m-HCC and nine p-HCC), 26 liver metastases and 16 liver hemangiomas. HCCs and liver metastases were diagnosed based on histology after liver resection or liver biopsy in all cases. Liver hemangioma was diagnosed by contrast-enhanced CT and/or MR imaging. The US equipment used in this study was SSA-770A (Aplio™XV; Toshiba Medical Systems Co., Otawara, Japan). The imaging mode was wideband harmonic imaging (commercially called Pulse subtraction) with transmission and reception frequencies of 3.75 MHz and 7.5 MHz, respectively. The contrast agent we used was SonoVue, which consists of sulfur hexafluoride microbubbles surrounded by phospholipids with a median diameter of 2.5 μm.

Computerized scheme for classification of FLLs

A series of image-processing steps in CAD, which basically consisted of three major parts, were as follows: (1) image data input and construction of processed images; (2) extraction of image feature values; and (3) application of ANNs and output for differential diagnosis. Please note that we simplified into three major steps (although six major steps were described in the referenced paper[32]).

Image data input and construction of processed images: After irrelevant information, such as patient names, IDs, and other symbols, was removed from the cine clips in the audio-video interleaving format as the input data, only continuous MFI images were reconstructed, and then four kinds of processed images were constructed. Figure 3A-H shows examples of the processed images. Image feature values were determined by use of the MFI image and the four processed images, and were used as input data for the CAD.

Extraction of image feature values: The image feature value is defined as the objective value by computer analysis of the subjective criteria that are used for diagnosing an FLL accurately in clinical practice, such as quick (slow) contrast-enhancement of an FLL, stronger (weaker) contrast enhancement of an FLL compared with liver parenchyma, and homogeneous (heterogeneous) contrast-enhancement of an FLL. For example, with regard to the speed of contrast enhancement, changes in average pixel values in an FLL are plotted against the time axis, and the slope (β value) is calculated. The steeper the slope, the faster the speed of contrast enhancement would be. Similarly, the maximum level of the average pixel value is compared between an FLL and a liver parenchyma for determining which region showed stronger contrast enhancement.

In this study, four kinds of major image feature values were used as CAD input data. Their image characteristics were as follows: (1) temporal feature; (2) morpho-

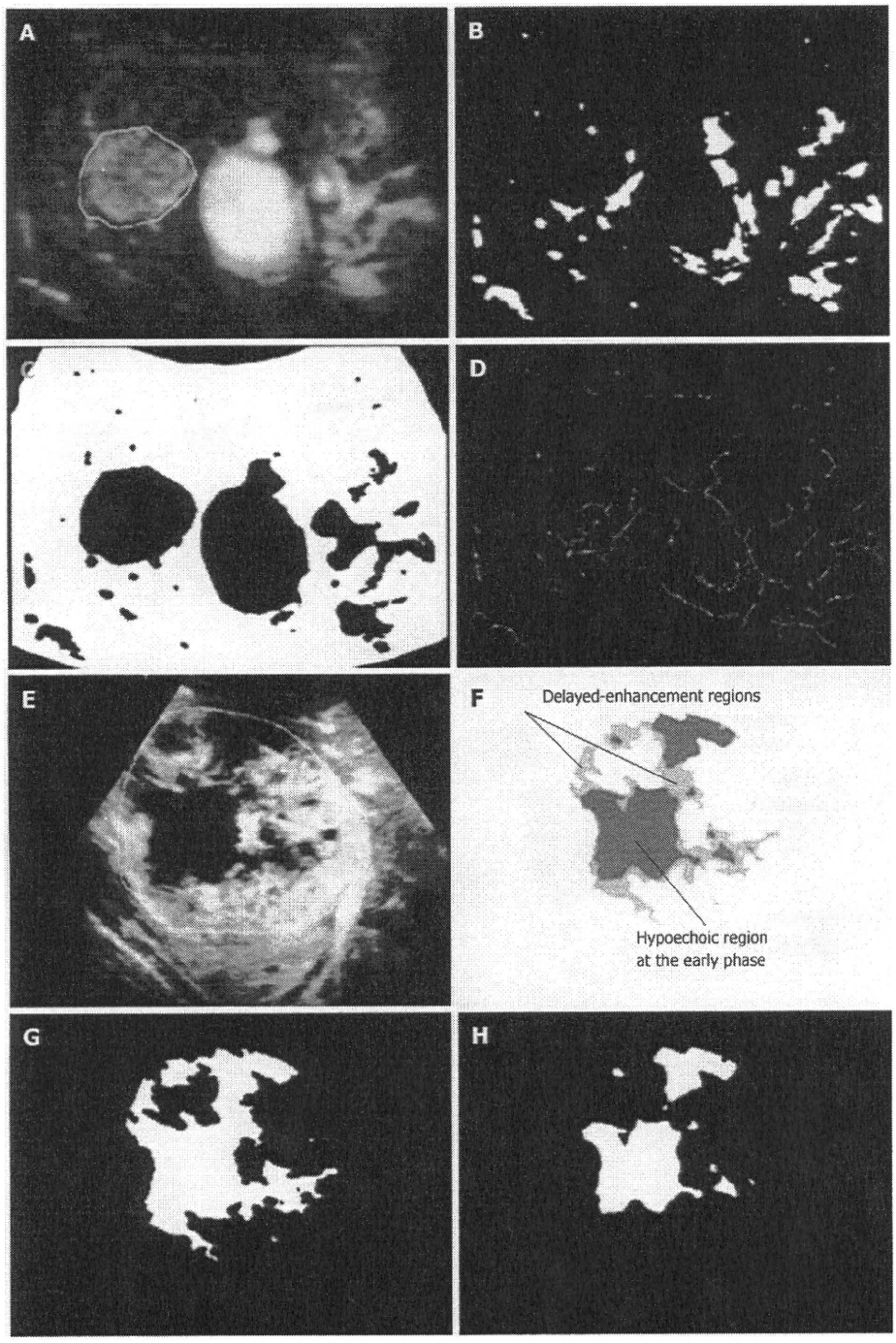

Figure 3 Extraction of morphologic and gray-level image features. A: Original MFI image at the early phase including one FLL (shown as the contour) and a portal vein; B: Vessel-like pattern enhanced image; C: Segmented adjacent liver parenchyma regions obtained from the original MFI image; D: Skeleton of vessel-like pattern enhanced image for estimating the average size of vessel-like patterns on the MFI image; Example of original MFI image at the delayed phase (E) and its segmented images for hyperechoic regions at the early (G) and delayed phase (H). The difference in the regions between two images at two phases was defined as delayed-enhancement region (F). Please note that we defined an "early phase" and a "delayed phase" in the MFI as a replenishment time for reaching 50% and 98% of the maximum average pixel value within a FLL, respectively. MFI: Micro-flow imaging. Reproduced, with modification, from Shiraishi *et al*[32], *Med Phys* 2008; 35: 1734-1746.

logic feature; (3) gray-level feature; and (4) features for a hypoechoic region. The details are shown in Table 3.

Feature 1 is an image feature value obtained from TIC, such as replenishment time, the peak pixel value, and the slope factor (β). In CEUS, for example, a hemangioma is characterized by a typical pattern, namely, a

Table 3 Image feature values used for CAD input data

Image feature values
Temporal features
Replenishment time (s)
Peak pixel value
Slope factor (β)
Morphologic features
Effective diameter of focal liver lesion
Average size of vessel-like patterns
Area ratio of vessel-like patterns
Gray-level features
Average pixel value with vessel-like patterns
Average pixel value without vessel-like patterns
Standard deviation of pixel value with vessel-like patterns
Standard deviation of pixel value without vessel-like patterns
Average pixel value ratio (focal liver lesion/adjacent liver parenchyma)
Average pixel value ratio (central/peripheral)
Features for hypoechoic region
Average pixel value
No. of hypoechoic regions
Area ratio of hypoechoic region
Difference in pixel value (delay-early)
Change in pixel value (delay-early)/s

Reproduced, with modification, from Shiraishi *et al*[32], *Med Phys* 2008; 35: 1734-1746.

peripheral globular enhancement with centripetal filling, whereas HCC and metastatic liver tumor are characterized by rapid contrast enhancement in an arterial phase. Use of the temporal feature as an image feature value, therefore, may be useful for differentiation of FLLs with different speeds of blood flow.

Feature 2 is an image feature value representing the morphologic characteristics of FLLs and intratumoral blood vessels, such as the effective diameter of an FLL, the average size of vessel-like patterns and the area ratio of vessel-like patterns. It has been reported that HCC with a larger tumor diameter exhibits poorer histological differentiation (i.e. higher percentages of p-HCC)[42], and thus the effective diameter of an FLL may be useful for diagnosis of histological grades of HCC. In addition, previous reports showed that the intratumoral vasculature visualized by MFI was dependent on the histological grade of HCC[39,41]. Thus, use of the morphologic image feature values obtained from the vessel-like pattern and the skeleton of a vessel-like pattern image may be useful for diagnosis of the histologic grade of HCC.

Feature 3 is an image feature value that represents tumor enhancement patterns, such as stronger contrast enhancement at the periphery of the tumor than at the center and at the tumor compared to the liver parenchyma. It has been reported that metastatic liver tumors often exhibit ring-like enhancement, and thus use of this image feature value may be useful for diagnosis of tumors with different contrast enhancement patterns.

Feature 4 is an image feature value that represents intratumoral heterogeneity in contrast enhancement. For example, spatial and temporal heterogeneity of a tumor in contrast enhancement can be evaluated by comparison

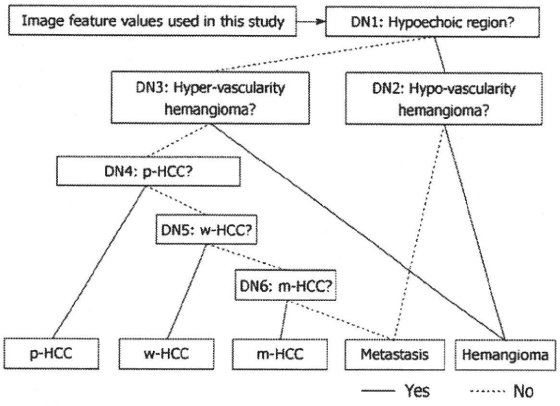

Figure 4 Illustration of the cascade of six artificial neural networks used in this. Six decisions in which alternative choices for specific groups of FLLs were determined by single ANN, leading a final diagnostic decision for five liver diseases.

of hypoechoic areas (no enhanced areas) between the MFI early-phase image and the MFI delayed-phase image. It has been reported that metastatic liver tumors and p-HCC often exhibit heterogeneous enhancement when compared with other liver tumors[38,43], and thus these image features may be useful for the differentiation of these tumors.

In order to select appropriate combinations of temporal and morphologic image features for each of the six ANNs, we used a stepwise method[44]. We thereby selected 16 temporal and morphologic image features, which were selected from 43 initial extracted features, and used them as input data for the six different ANNs for making decisions at each decision step in the cascade.

Application of ANNs and output for differential diagnosis: In the CAD, image feature values extracted from MFI images were used for input data for ANNs. We used parameters in the ANNs to learn the relationship between the repeated presentation of input data in random order and their corresponding output "teacher" data. Our ANNs were constructed with the stratified six different ANNs in order to classify "unknown" FLL input into one of five types of liver diseases (e.g. w-HCC, m-HCC, p-HCC, liver metastasis and liver hemangioma).

All decisions in each of the stratified six different ANNs, shown in Figure 4, were determined using a two-alternative choice. The six decisions used in the six ANNs were determined as follows: (1) D1: Does this lesion have hypoechoic regions (yes) or not (no)? (2) D2: Is this lesion a hypovascular hemangioma (yes) or a hypovascularity metastasis (no)? (3) D3: Is this lesion a hypervascular hemangioma (yes) or other (no)? (4) D4: Is this lesion a p-HCC (yes) or other (no)? (5) D5: Is this lesion a w-HCC (yes) or other (no)? and (6) D6: Is this lesion a m-HCC (yes) or a hypervascular metastasis (no)?

A set of image feature values was selected for each ANN, and learning processes and tests were carried out independently. In learning and testing tasks with ANNs,

Table 4 Performance of CAD scheme for classification in five categories using computerized scheme *n* (%)

Lesion	*n*	Classification with CAD				
		HCC			Metastasis	Hemangioma
		w-HCC	m-HCC	p-HCC		
Total	103					
w-HCC	24	19 (79.2)	1 (4.2)	2 (8.3)	2 (8.3)	0 (0.0)
m-HCC	28	5 (17.9)	14 (50.0)	4 (14.3)	3 (10.7)	2 (7.1)
P-HCC	9	1 (11.1)	0 (0.0)	7 (77.8)	1 (11.1)	0 (0.0)
Metastasis	26	2 (7.7)	1 (3.8)	0 (0.0)	23 (88.5)	0 (0.0)
Hemangioma	16	0 (0.0)	0 (0.0)	0 (0.0)	1 (6.3)	15 (93.8)

Overall diagnostic accuracy: 78/103 (75.7%). CAD performance was evaluated by a leave-one-case-out methods.Reproduced, with modification, from Shiraishi *et al*[32], *Med Phys* 2008; 35: 1734-1746.

the leave-one-out test method was employed in individual ANNs.

The classification accuracies for each type of FLL and also for all 103 FLLs were determined with percentages (%) of correctly classified cases among the total number of cases.

CAD results

Table 4 shows the performance of the computerized scheme for the classification of five types of FLLs (w-HCCs, m-HCCs, p-HCCs, metastases and hemangiomas). The classification accuracies for the 103 FLLs were 88.5% for metastasis, 93.8% for hemangioma, 79.2% for w-HCC, 50.0% for m-HCC and 77.8% for p-HCC. When the classification was done for three types of FLLs (HCCs, metastasis and hemangioma), the classification accuracies for all HCCs was 86.9%. The average classification accuracies for three and five types of FLLs were 88.3% and 75.7%, respectively.

PRACTICAL ISSUES IN CAD AND PERSPECTIVES FOR THE FUTURE

In general, a reliable image database is indispensable for research and development of CAD. In particular, an appropriate number of clinical cases should be used, and attention must be paid to the detection and/or characterization of lesions contained in the images and to the degrees of diagnostic difficulty. For development of a CAD scheme that will become available for clinical application, cases in the database should include various degrees of difficulty in diagnosis, from relatively easy to markedly difficult. Furthermore, the liver is the largest organ in the human body and part of the liver is protected by ribs. Unlike CT and MR imaging, it is therefore difficult to scan the whole liver by US[45]. In addition, US scanning can be difficult in cases of severe obesity. These factors seem to interfere with US on the liver, and also CAD for US on the liver.

One of the most critical components for research on CAD is software development. To this end, programming technology, image processing and knowledge of information processing are required. In general, however, physicians have insufficient knowledge of these skills, and thus close collaboration with physicists is required. On the other hand, it is difficult for software to be developed by physicists alone, because they have insufficient medical knowledge about diagnosis and detection. Therefore, close collaboration with physicians is also necessary.

As a characteristic of CAD, it would be useful if CAD could detect and/or characterize lesions that physicians are likely to overlook and/or misdiagnose, even if the performance of CAD is not highly accurate; and conversely, CAD would not be useful if physicians do not believe the results even when correct. Thus, once the algorithm of CAD is developed, its objective evaluation is necessary. To date, however, no paper on CAD in the liver has included an objective evaluation of the performance of CAD. An observer performance study is a representative evaluation method; observers are required to carry out evaluations under two conditions, with and without the results of computer analysis. Receiver operating characteristic curves can then be obtained based on the results for evaluation of the performance of CAD.

In addition, when the results of evaluation are satisfactory, based on the database in the laboratory, it is necessary to carry out practical tests on a number of unexplored clinical cases as the next step. It is also necessary to develop a practical CAD prototype system and to install it in the workplace in the hospital for a prospective clinical trial. To this end, cooperation by the hospital and physicians would be required for reliable evaluation.

Eventually, to reap the advantages of CAD, commercialization by companies is required. When equipment, systems and software applicable for clinical practice become available commercially, they can be used in hospitals worldwide.

CONCLUSION

In this article, we provided an overview of CAD based on US in the liver. Moreover, we introduced two different types of CAD schemes with CEUS images aimed at the differential diagnosis of FLLs.

The performance of our CAD system for the classification of FLLs could be considered as comparable to those reported by Wilson *et al*[9]. Although their report

was not on results of CAD, their algorithm used subjective assessment of physicians for information on portal venous enhancement for the distinction between benign and malignant FLLs, and their results indicated a high classification accuracy (i.e. 92% for benign and 93% for malignant FLLs).

As shown in this article, the diagnostic accuracies of CAD based on the results of physicians' subjective pattern classification could be considered as comparable to those of CAD based on a computerized scheme. Interestingly, the former CAD was, however, superior to the latter in the diagnosis of three types of FLLs (i.e. HCCs, metastasis, and hemangioma; 94.2% *vs* 88.3%). In contrast, the latter was superior to the former in the diagnosis of five types of FLLs (w-HCCs, m-HCCs, p-HCCs, metastases and hemangiomas; 75.7% *vs* 71.5%). These results suggest that human observers might differ in determining feature values from a computer in the diagnosis of FLLs. Thus, if we take advantage of computer outputs, diagnostic accuracy could be greatly improved.

In our present studies, to establish CAD for FLLs, we used temporal and morphologic features, including physicians' subjective pattern classifications, as image features of FLLs on the contrast-enhancement patterns in the arterial phase of CEUS. However, we did not use findings from portal and late phases (i.e. the presence or absence of washout) as image features of our CADs. That is because, as it is now, it is difficult to recognize automatically all of the data in a dynamic-imaging series for input data because of the problem of the timing of patient breath holding.

Our CAD results showed that the accuracy of m-HCC in both CADs was quite low (subjective analysis: 41.7% and quantitative analysis: 50.0%). This can be related to the fact that we did not use portal and late phase images as input data of CADs, because both w-HCC and m-HCC frequently show arterial enhancement in the same fashion. It is a principal limitation of our CADs. Thus, if our CAD schemes would have portal and late phase information, the performance of our CADs would be much more improved. Our future work should be to recognize hole ultrasonographic image data (i.e. wash-in and wash-out information) automatically as input data to the CAD system.

The other limitation is that focal nodular hyperplasia (FNH) and hepatocellular adenoma were not included in these studies. Both FNH and hepatic adenoma tend to have FLLs presenting a hypervascular pattern in the arterial phase, and it can be difficult to distinguish from HCC, liver metastasis, and hemangioma. However, Kim *et al*[46] reported that monitoring the direction of early arterial filling or the vascular morphology continuously by CEUS enable one to differentiate, to some extent, among FLLs with hypervascularity, including FNH, hemangioma, HCCs, or metastases. However, hepatic adenoma lacks characteristic features even with CEUS, and differentiation of hepatic adenoma from other plethoric FLLs has been reported to be difficult. Hepatocellular adenoma is rare tumor, and therefore it seems extremely rare for this tumor to become a subject of differential diagnosis.

ACKNOWLEDGMENTS

The authors are grateful to Mrs. Elisabeth Lanzl for improving the manuscript.

REFERENCES

1 **Kitzman DW**, Goldman ME, Gillam LD, Cohen JL, Aurigemma GP, Gottdiener JS. Efficacy and safety of the novel ultrasound contrast agent perflutren (definity) in patients with suboptimal baseline left ventricular echocardiographic images. *Am J Cardiol* 2000; **86**: 669-674
2 **Leen E**, Angerson WJ, Yarmenitis S, Bongartz G, Blomley M, Del Maschio A, Summaria V, Maresca G, Pezzoli C, Llull JB. Multi-centre clinical study evaluating the efficacy of SonoVue (BR1), a new ultrasound contrast agent in Doppler investigation of focal hepatic lesions. *Eur J Radiol* 2002; **41**: 200-206
3 **Krix M**, Kiessling F, Essig M, Herth F, Karcher A, Le-Huu M, Kauczor HU, Delorme S. Low mechanical index contrast-enhanced ultrasound better reflects high arterial perfusion of liver metastases than arterial phase computed tomography. *Invest Radiol* 2004; **39**: 216-222
4 **Maruyama H**, Matsutani S, Saisho H, Mine Y, Yuki H, Miyata K. Different behaviors of microbubbles in the liver: time-related quantitative analysis of two ultrasound contrast agents, Levovist and Definity. *Ultrasound Med Biol* 2004; **30**: 1035-1040
5 **Gaiani S**, Celli N, Piscaglia F, Cecilioni L, Losinno F, Giangregorio F, Mancini M, Pini P, Fornari F, Bolondi L. Usefulness of contrast-enhanced perfusional sonography in the assessment of hepatocellular carcinoma hypervascular at spiral computed tomography. *J Hepatol* 2004; **41**: 421-426
6 **Burns PN**, Wilson SR, Simpson DH. Pulse inversion imaging of liver blood flow: improved method for characterizing focal masses with microbubble contrast. *Invest Radiol* 2000; **35**: 58-71
7 **Albrecht T**, Hoffmann CW, Schettler S, Overberg A, Ilg M, von Behren PL, Bauer A, Wolf KJ. B-mode enhancement at phase-inversion US with air-based microbubble contrast agent: initial experience in humans. *Radiology* 2000; **216**: 273-278
8 **Kim AY**, Choi BI, Kim TK, Kim KW, Lee JY, Han JK. Comparison of contrast-enhanced fundamental imaging, second-harmonic imaging, and pulse-inversion harmonic imaging. *Invest Radiol* 2001; **36**: 582-588
9 **Wilson SR**, Burns PN. An algorithm for the diagnosis of focal liver masses using microbubble contrast-enhanced pulse-inversion sonography. *AJR Am J Roentgenol* 2006; **186**: 1401-1412
10 **Wilson SR**, Burns PN. Liver mass evaluation with ultrasound: the impact of microbubble contrast agents and pulse inversion imaging. *Semin Liver Dis* 2001; **21**: 147-159
11 **Eckersley RJ**, Chin CT, Burns PN. Optimising phase and amplitude modulation schemes for imaging microbubble contrast agents at low acoustic power. *Ultrasound Med Biol* 2005; **31**: 213-219
12 **Leavens C**, Williams R, Foster FS, Burns PN, Sherar MD. Golay pulse encoding for microbubble contrast imaging in ultrasound. *IEEE Trans Ultrason Ferroelectr Freq Control* 2007; **54**: 2082-2090
13 **Harvey CJ**, Blomley MJ, Eckersley RJ, Cosgrove DO, Patel N, Heckemann RA, Butler-Barnes J. Hepatic malignancies: improved detection with pulse-inversion US in late phase of enhancement with SH U 508A-early experience. *Radiology* 2000; **216**: 903-908
14 **Gruszauskas NP**, Drukker K, Giger ML, Chang RF, Sennett CA, Moon WK, Pesce LL. Breast US computer-aided diagnosis system: robustness across urban populations in South Korea and the United States. *Radiology* 2009; **253**: 661-671
15 **Drukker K**, Gruszauskas NP, Sennett CA, Giger ML. Breast US computer-aided diagnosis workstation: performance with a large clinical diagnostic population. *Radiology* 2008; **248**: 392-397
16 **Wu WJ**, Moon WK. Ultrasound breast tumor image comput-

er-aided diagnosis with texture and morphological features. *Acad Radiol* 2008; **15**: 873-880
17 **Shen WC**, Chang RF, Moon WK. Computer aided classification system for breast ultrasound based on Breast Imaging Reporting and Data System (BI-RADS). *Ultrasound Med Biol* 2007; **33**: 1688-1698
18 **Sahiner B**, Chan HP, Roubidoux MA, Hadjiiski LM, Helvie MA, Paramagul C, Bailey J, Nees AV, Blane C. Malignant and benign breast masses on 3D US volumetric images: effect of computer-aided diagnosis on radiologist accuracy. *Radiology* 2007; **242**: 716-724
19 **Chen CM**, Chou YH, Han KC, Hung GS, Tiu CM, Chiou HJ, Chiou SY. Breast lesions on sonograms: computer-aided diagnosis with nearly setting-independent features and artificial neural networks. *Radiology* 2003; **226**: 504-514
20 **Doi K**, Giger ML, Nishikawa RM, Hoffmann KR, MacMahon H, Schmidt RA, Chua KG. Digital radiography. A useful clinical tool for computer-aided diagnosis by quantitative analysis of radiographic images. *Acta Radiol* 1993; **34**: 426-439
21 **Doi K**, MacMahon H, Katsuragawa S, Nishikawa RM, Jiang Y. Computer-aided diagnosis in radiology: potential and pitfalls. *Eur J Radiol* 1999; **31**: 97-109
22 **Doi K**. Current status and future potential of computer-aided diagnosis in medical imaging. *Br J Radiol* 2005; **78** Spec No 1: S3-S19
23 **Abe H**, MacMahon H, Engelmann R, Li Q, Shiraishi J, Katsuragawa S, Aoyama M, Ishida T, Ashizawa K, Metz CE, Doi K. Computer-aided diagnosis in chest radiography: results of large-scale observer tests at the 1996-2001 RSNA scientific assemblies. *Radiographics* 2003; **23**: 255-265
24 **Gur D**, Zheng B, Fuhrman CR, Hardesty L. On the testing and reporting of computer-aided detection results for lung cancer detection. *Radiology* 2004; **232**: 5-6
25 **Lodwick GS**, Haun CL, Smith WE, Keller RF, Robertson ED. Computer diagnosis of primary bone tumors: a preliminary report. *Radiology* 1963; **80**: 273-275
26 **Meyers PH**, Nice CM Jr, Becker HC, Nettleton WJ JR, Sweeney JW, Meckstroth GR. Automated computer analysis of radiographic images. *Radiology* 1964; **83**: 1029-1034
27 **Winsberg F**, Elkin M, Macy J, Bordaz V, Weymouth W. Detection of radiographic abnormalities in mammograms by means of optical scanning and computer analysis. *Radiology* 1967; **89**: 211-215
28 **Li G**, Luo Y, Deng W, Xu X, Liu A, Song E. Computer aided diagnosis of fatty liver ultrasonic images based on support vector machine. *Conf Proc IEEE Eng Med Biol Soc* 2008; **2008**: 4768-4771
29 **Thijssen JM**, Starke A, Weijers G, Haudum A, Herzog K, Wohlsein P, Rehage J, De Korte CL. Computer-aided B-mode ultrasound diagnosis of hepatic steatosis: a feasibility study. *IEEE Trans Ultrason Ferroelectr Freq Control* 2008; **55**: 1343-1354
30 **Jeong JW**, Lee S, Lee JW, Yoo DS, Kim S. The echotextural characteristics for the diagnosis of the liver cirrhosis using the sonographic images. *Conf Proc IEEE Eng Med Biol Soc* 2007; **2007**: 1343-1345
31 **Sugimoto K**, Shiraishi J, Moriyasu F, Doi K. Computer-aided diagnosis of focal liver lesions by use of physicians' subjective classification of echogenic patterns in baseline and contrast-enhanced ultrasonography. *Acad Radiol* 2009; **16**: 401-411
32 **Shiraishi J**, Sugimoto K, Moriyasu F, Kamiyama N, Doi K. Computer-aided diagnosis for the classification of focal liver lesions by use of contrast-enhanced ultrasonography. *Med Phys* 2008; **35**: 1734-1746
33 **Huang-Wei C**, Bleuzen A, Olar M, Portalez D, Roumy J, Trillaud H, Tranquart F. Role of parametric imaging in contrast-enhanced sonography of hepatic focal nodular hyperplasia. *J Clin Ultrasound* 2006; **34**: 367-373
34 **Huang-Wei C**, Bleuzen A, Bourlier P, Roumy J, Bouakaz A, Pourcelot L, Tranquart F. Differential diagnosis of focal nodular hyperplasia with quantitative parametric analysis in contrast-enhanced sonography. *Invest Radiol* 2006; **41**: 363-368
35 **Ishizawa T**, Yamamoto T, Sekikawa T. The diagnostic values of measuring the liver volume in detecting occult hepatic metastases from colorectal cancer. *Hepatogastroenterology* 2007; **54**: 514-517
36 **Gilja OH**, Hausken T, Berstad A, Odegaard S. Measurements of organ volume by ultrasonography. *Proc Inst Mech Eng H* 1999; **213**: 247-259
37 **Itai Y**, Ohtomo K, Ohnishi S, Atomi Y, Itoh T, Fukuhisa K, Iinuma T. Ultrasonography of small hepatic tumors. *Radiat Med* 1987; **5**: 14-19
38 **Quaia E**, Calliada F, Bertolotto M, Rossi S, Garioni L, Rosa L, Pozzi-Mucelli R. Characterization of focal liver lesions with contrast-specific US modes and a sulfur hexafluoride-filled microbubble contrast agent: diagnostic performance and confidence. *Radiology* 2004; **232**: 420-430
39 **Sugimoto K**, Moriyasu F, Kamiyama N, Metoki R, Yamada M, Imai Y, Iijima H. Analysis of morphological vascular changes of hepatocellular carcinoma by microflow imaging using contrast-enhanced sonography. *Hepatol Res* 2008; **38**: 790-799
40 **Wilson SR**, Jang HJ, Kim TK, Iijima H, Kamiyama N, Burns PN. Real-time temporal maximum-intensity-projection imaging of hepatic lesions with contrast-enhanced sonography. *AJR Am J Roentgenol* 2008; **190**: 691-5
41 **Yang H**, Liu GJ, Lu MD, Xu HX, Xie XY. Evaluation of the vascular architecture of hepatocellular carcinoma by micro flow imaging: pathologic correlation. *J Ultrasound Med* 2007; **26**: 461-467
42 **Fan ZH**, Chen MH, Dai Y, Wang YB, Yan K, Wu W, Yang W, Yin SS. Evaluation of primary malignancies of the liver using contrast-enhanced sonography: correlation with pathology. *AJR Am J Roentgenol* 2006; **186**: 1512-1519
43 **Jang HJ**, Kim TK, Burns PN, Wilson SR. Enhancement patterns of hepatocellular carcinoma at contrast-enhanced US: comparison with histologic differentiation. *Radiology* 2007; **244**: 898-906
44 **Hocking RR**. The analysis and selection of variables in linear regression. *Biometrics* 1976; **32**: 1-49
45 **Sugimoto K**, Shiraishi J, Moriyasu F, Saito K, Doi K. Improved detection of hepatic metastases with contrast-enhanced low mechanical-index pulse inversion ultrasonography during the liver-specific phase of sonazoid: observer performance study with JAFROC analysis. *Acad Radiol* 2009; **16**: 798-809
46 **Kim TK**, Jang HJ, Burns PN, Murphy-Lavallee J, Wilson SR. Focal nodular hyperplasia and hepatic adenoma: differentiation with low-mechanical-index contrast-enhanced sonography. *AJR Am J Roentgenol* 2008; **190**: 58-66

S- Editor Cheng JX **L- Editor** Lutze M **E- Editor** Zheng XM

JOURNAL OF MAGNETIC RESONANCE IMAGING 32:229–234 (2010)

Technical Note

Effect of Gd-EOB-DTPA on T2-Weighted and Diffusion-Weighted Images for the Diagnosis of Hepatocellular Carcinoma

Kazuhiro Saito, MD,[1]* Yoichi Araki, RT,[1] Jinho Park, MD,[1] Ryo Metoki, MD,[2] Hiroaki Katsuyama, RT,[1] Ryota Nishio, MD,[1] Dai Kakizaki, MD,[1] Fuminori Moriyasu, MD,[2] and Koichi Tokuuye, MD[1]

Purpose: To evaluate the effect of gadolinium ethoxybenzyl diethylenetriamine pentaacetic acid (Gd-EOB-DTPA) on T2-weighted imaging (T2WI) and diffusion-weighted imaging (DWI) for the diagnosis of hepatocellular carcinoma (HCC).

Materials and Methods: The phantom signal intensity was measured. We also evaluated 72 patients including 30 patients with HCC. T2WI and DWI were obtained before and then 4 and 20 min after injecting the contrast medium. The signal to noise ratio (SNR), contrast to noise ratio (CNR), and apparent diffusion coefficient (ADC) were calculated in the tumor and liver parenchyma.

Results: The phantom signal intensity increased on T2WI at a concentration of contrast medium less than 0.2 mmol/L but decreased when the concentration exceeded 0.4 mmol/L. SNR of the liver parenchyma on T2WI was significantly different between before and 4 min after injecting the contrast medium, while there were no significant differences between before and 4 and 20 min after injection. On T2WI, SNR, and CNR of HCC showed no significant differences at any time. SNR, CNR, and ADC of the liver parenchyma and tumor on DWI also showed no significant differences at any time.

Conclusion: It is acceptable to perform T2WI and DWI after injection of Gd-EOB-DTPA for the diagnosis of HCC.

Key Words: Gd-EOB-DTPA; Primovist; hepatocellular carcinoma; T2-weighted image; diffusion-weighted image
J. Magn. Reson. Imaging 2010;32:229–234.

GADOLINIUM ETHOXYBENZYL DIETHYLENETRIAMINE PENTAACETIC acid (Gd-EOB-DTPA, Primovist®, Bayer-Schering, Osaka, Japan) is a liver-specific contrast medium. It enables dynamic studies with a bolus injection similar to a nonspecific extracellular contrast medium (1,2). This contrast medium accumulates in hepatocytes and is excreted into the bile; therefore, there is a T1 shortening effect in the liver parenchyma. The hepatobiliary phase begins 1.5 min after injecting the contrast medium and continues for 2 h, and the peak liver signal intensity is obtained 20 min after injecting the contrast medium (2). In general, the contrast medium accumulates only slightly in the tumor, and hence, the tumor is depicted as a hypointense image compared with the surrounding liver parenchyma at 20 min after injection (3). Therefore, it is essential to wait for 20 min after administering the injection for liver parenchymal enhancement (2,4). However, a 20-min wait causes throughput decline. If T2-weighted images (T2WI) and diffusion-weighted images (DWI) could be performed within the initial 20 min, the examination time can be shortened and throughput can be improved (5).

The effect of a nonspecific extracellular contrast medium on T2WI is reportedly small (6,7); however, there are few reports concerning Gd-EOB-DTPA (8). Recently, the usefulness of DWI has been reported for both detection of liver tumors and evaluation of therapeutic outcomes (9,10). The effect of a nonspecific extracellular contrast medium on DWI has also been reported to be small (11). However, there are no reports on the effects of Gd-EOB-DTPA. Thus, we evaluated the effects of Gd-EOB-DTPA on both T2WI and DWI by conducting phantom and clinical studies in patients with and without hepatocellular carcinoma (HCC).

MATERIALS AND METHODS

Images were acquired using an Avanto 1.5 Tesla (T) super conduction system (Siemens, Erlangen, Germany) and an eight-channel phased-array body matrix coil. The maximum gradient strength was 45 T/m.

Phantom Study

Different concentrations of Primovist in water were placed in the phantom and T2WI and DWI were

[1]Department of Radiology, Tokyo Medical University, Tokyo, Japan.
[2]Department of Gastroenterology and Hepatology, Tokyo Medical University, Tokyo, Japan.
*Address reprint requests to: K.S., 6-7-1 Nishi-Shinjuku, Shinjuku-ku, Tokyo, Japan. E-mail: saito-k@tokyo-med.ac.jp
Received July 7, 2009; Accepted April 1, 2010.
DOI 10.1002/jmri.22219
Published online in Wiley InterScience (www.interscience.wiley.com).

performed using the parameters that are used clinically. The diluted concentrations were 0.05, 0.1, 0.2, 0.4, 0.6, 0.8, 1.0, and 2.0 mmol/L. The T2WI parameters were as follows: repetition time/echo time (TR/TE), 3600/99 ms; flip angle, 150°; 1 averaging; matrix, 256 × 75%; echo train length, 29; slice thickness, 6 mm; slice gap, 1.2 mm; acquisition time, 14 s. The DWI parameters were as follows: TR/TE, 1600/66 ms; flip angle, 150°; 2 averaging; matrix, 128 × 100%; echo train length, 29; slice thickness, 6 mm; slice gap, 1.2 mm; acquisition time, 24 seconds; b values, 100 and 800. The signal intensity of each phantom was measured.

Clinical Evaluation

Subjects

We studied 90 consecutive patients during a 6-month period (April 2008–September 2008). Primovist-enhanced MRI was used to evaluate their liver lesions. Exclusion criteria were cases of instability during breathholding, interruption of examination due to machine trouble, nausea, and difficulty in measuring signal intensity in the normal liver parenchyma because of replacement by large/many tumors or portal invasion. Finally, 72 patients were chosen for this study. Our institutional review board approved this prospective study, and informed consent was obtained from all patients. The subjects consisted of 44 men and 28 women. Their mean age was 67.3 ± 11.0 years (mean ± standard deviation). In 59 patients, chronic liver damage was due to type-B (n = 7), type-C (n = 44), or type-B and C (n = 1) hepatitis; alcoholic hepatitis (n = 4); primary biliary cirrhosis (n = 1); and unknown reason (n = 2), whereas 13 patients had no chronic liver disease. Two patients with chronic type-C hepatitis also had fatty liver. The series included 30 patients with HCC. In patients having more than one lesion, we chose the largest lesion to study. The mean tumor size was 20.8 ± 9.4 mm. There were 16 pathologically proven lesions (14 through biopsies and 2 by means of operations), and the remaining 14 were diagnosed by imaging. The pathologically proven lesions included 4 well-differentiated, 7 moderately differentiated, and 5 poorly differentiated HCCs. The criteria for HCC diagnosis by imaging were a tumor stain in the arterial phase, hypodensity or hypointensity in the equilibrium phase on dynamic computed tomography (CT) or MRI, and a lesion diameter of over 10 mm with an increased α-fetoprotein level (12).

We also performed angiography-assisted CT, and the findings of these lesions were a tumor stain on CT hepatic arteriography and a perfusion defect on CT during arterioportography (13).

Imaging

T1-weighted images (T1WI) included in-phase and opposed-phase images; T2WI and DWI were obtained before injecting Primovist. The T1WI parameters (in-phase and opposed-phase) were as follows: TR/TE, 120/4.76, 2.38 ms; flip angle, 75°; 1 averaging; matrix, 256 × 140%; PAT factor, 2; slice thickness, 6 mm; slice gap, 1.2 mm; acquisition time, 13 s. Primovist (0.025 μmol/kg) was injected by means of the antecubital vein at 2 or 3 mL/s followed by 20 mL of physiological saline. The dynamic study included the arterial phase, portal phase, and 4 min after injection of the contrast medium. A three-dimensional volumetric interpolated breathhold examination (3D-VIBE) was performed along with the dynamic study. The 3D-VIBE parameters were as follows: TR/TE, 4.28/1.78 ms; flip angle, 15°; matrix, 256 × 85%; PAT factor, 2; slice thickness, 3 mm; acquisition time, 20 s. T2WI and DWI were performed immediately after the dynamic study. The hepatobiliary phase was obtained 20 min after injecting the contrast medium with 3D-VIBE, and T2WI and DWI were performed again immediately after obtaining the hepatobiliary phase. The patients wore the receiving coil throughout the examination. The breathhold method was adopted for T2WI and DWI. The parameters for this examination were the same as those of the phantom study.

Quantitative Analysis

The regions of interest (ROI) to measure signal intensity were the liver parenchyma and tumor. Liver parenchyma signal intensity was measured three times at different points on the right lobe (avoiding vasculature) and their average was obtained. Tumor signal intensity was measured once, and the ROI was set to contain as much of the lesion as possible. In this study, none of the tumors included a necrotic area. Signal intensity measurement was performed by a radiologist (with 9 years of experience) whose specialty was abdominal imaging. The measurement was performed on the same region for each imaging procedure with reference to the anatomical structure.

The signal to noise ratio (SNR), contrast to noise ratio (CNR), and apparent diffusion coefficient (ADC) of the liver parenchyma and tumor before and 4 and 20 min after injection of the contrast medium were calculated using the following formula: SNR (liver) = signal intensity of liver parenchyma/standard deviation of the background noise. SNR (tumor) = signal intensity of tumor/standard deviation of tumor. CNR = (signal intensity of tumor − signal intensity of liver parenchyma)/standard deviation of the background noise. ADC = log [SI (b1)/SI (b2)]/[(b2) − (b1)], where b1: 100; b2: 800; SI (b1): signal intensity of b = 100; SI (b2): signal intensity of b = 800. The presence of a significant change in SNR and ADC values of the liver and HCC and CNR were evaluated. CNR was evaluated in all types of differentiated tumors.

Qualitative Analysis

Thirty HCC samples were qualitatively evaluated by three observers. Two observers were experienced radiologists (with 16 and 18 years of experience), and the third one was a physician whose specialty was liver imaging (with 9 years of experience). The coordinator saved each HCC image in the computer. They displayed the same image slice level in the hepatobiliary phase, T2WI, and DWI at the same time on a monitor.

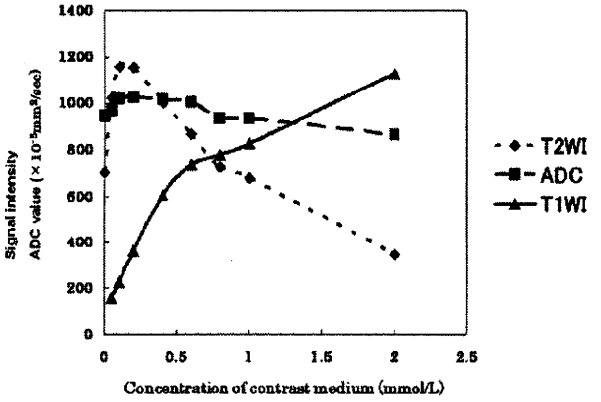

Figure 1. The graph shows signal intensity and ADC values of the phantom with various concentrations of Primovist. T2 relaxation was observed at concentrations of 0.2 mmol/L, and T2-weighted image signal intensity decreased at concentrations ≥0.4 mmol/L. The changes in ADC values were small regardless of concentration.

We used the DWI with b factor = 800. The T2WI and DWI had the same delay time and were displayed together. The coordinator indicated the lesion with an arrow on the hepatobiliary phase image. In all, 90 sets of images were selected at random, and three observers evaluated each image independently, classifying them into four categories: 1, no depiction; 2, possible depiction; 3, usual depiction; 4, clear depiction (equal to spleen). Each observer was aware of the presence of an HCC lesion on the image.

Statistical Analysis

We used a repeated-measures analysis of variance (ANOVA) for quantitative analysis. Qualitative analysis was performed using the Freidman test. A *P* value of less than 0.05 indicated a statistically significant difference. Interobserver variability was evaluated using the kappa value to measure the degree of agreement. A kappa value of 0.2 or less was regarded as slight agreement, 0.21 to 0.40 as fair, 0.41 to 0.60 as moderate, 0.61 to 0.80 as substantial, and 0.81 or more as almost perfect. Statistical analysis was performed using SPSS version 16.0 for Windows.

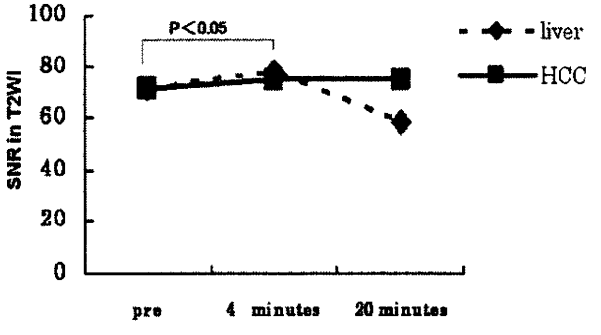

Figure 2. SNR of the liver and HCC. A significant difference is observed between the SNR of the liver on the in precontrast T2-weighted image and 4 min after contrast-enhanced T2-weighted image.

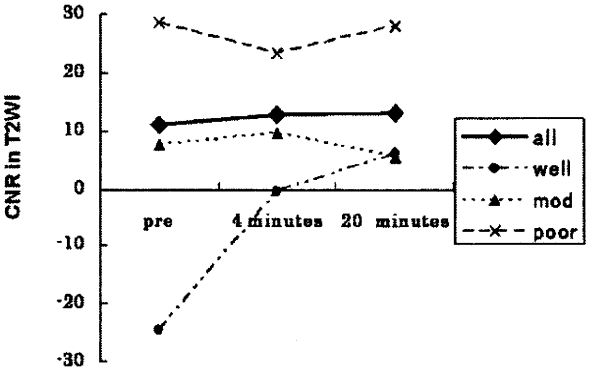

Figure 3. There was no significant difference in CNR between pre- and postenhanced T2-weighted images.

RESULTS

Phantom Study

The results of the phantom study are shown in Figure 1. The phantom signal intensity increased on T2WI at a concentration of contrast medium less than 0.2 mmol/L but decreased when the concentration exceeded 0.4 mmol/L. The change in ADC value was slight on DWI regardless of the concentration of contrast medium.

Clinical Evaluation

Quantitative Analysis

SNRs of the liver parenchyma were 71.0, 78.4, and 58.3 on T2WI before and 4 and 20 min after injecting the contrast medium, respectively. There were significant differences between before and 4 min after the injection of contrast medium ($P < 0.05$). SNRs of HCCs were 71.1, 74.2, and 74.8 on T2WI before and 4 and 20 min after injecting the contrast medium, respectively. There were no significant differences at any time ($P > 0.05$) (Fig. 2). CNR of the HCC were 11.2, 12.8, and 13.1 before and 4 and 20 min after injecting the contrast medium, respectively. There were no significant differences at any time ($P > 0.05$) (Fig. 3). CNR of each differentiated HCC were as follows: well-differentiated, −24.6, −0.3, and 6.1; moderately differentiated, 7.7, 9.6, and 5.5; poorly differentiated, 28.7, 23.3, and 28.0 before and 4 and 20 min after injecting the contrast medium, respectively (Fig. 3). CNR of well-differentiated HCC tended to increase, but no significant difference between before and after enhancement for all differentiated HCC was observed.

SNRs of the liver parenchyma on DWI with b = 100 were 107.7, 115.3, and 107.7 before and 4 and 20 min after injecting the contrast medium, respectively, and those of b = 800 were 57.1, 58.9, and 58.4, respectively. There were no significant differences between before and after enhancement ($P > 0.05$). SNRs of HCC on DWI with b = 100 were 140.1,

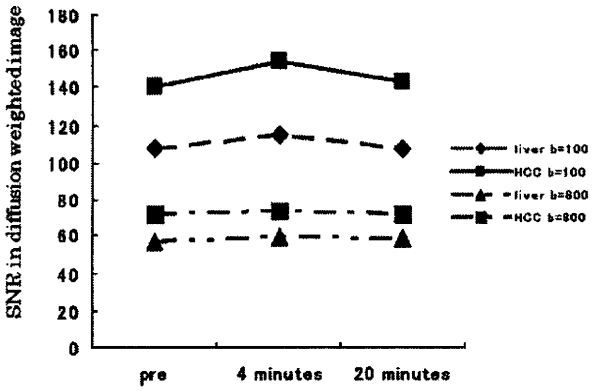

Figure 4. There was no significant difference in SNR of the liver and HCC between pre- and postenhanced diffusion-weighted images.

153.7, and 143.2 before and 4 and 20 min after injecting the contrast medium, respectively, and those of b = 800 were 72.1, 73.7, and 71.8, respectively. SNRs of HCC for both b values showed no significant differences between before and after enhancement ($P > 0.05$) (Fig. 4). CNRs of HCC on DWI with b = 100 were 32.4, 38.4, and 35.5 before and 4 and 20 min after injection of contrast medium, respectively, and those with b = 800 were 13.4, 14.8, and 13.4, respectively. Thus, CNR showed no significant difference between before and after enhancement ($P > 0.05$) (Fig. 5). CNR of each differentiated HCC on DWI with b = 100 were as follows: well-differentiated, 53.0, 76.0, and 72.9; moderately differentiated, 32.0, 39.0, and 39.0; and poorly differentiated, 61.6, 61.9, and 58.9 before and 4 and 20 min after injecting the contrast medium, respectively, and those with b = 800 were as follows: well-differentiated, 26.8, 29.6, and 24.2; moderately differentiated, 19.6, 18.1, and 21.3; and poorly differentiated, 31.6, 32.0, and 27.6, respectively (Fig. 5). There was no significant difference in CNR between before and after enhancement for all differentiated HCCs.

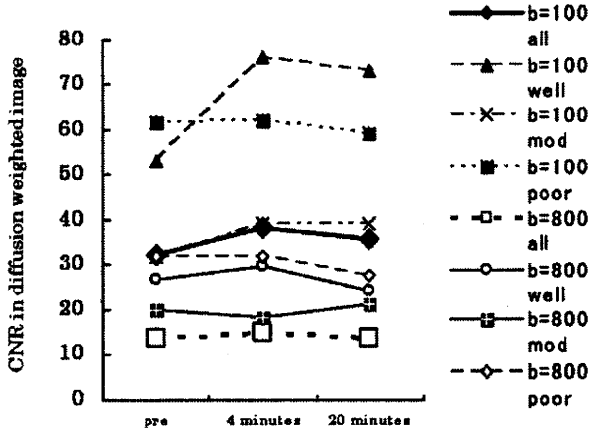

Figure 5. There was no significant difference in CNR between pre- and postenhanced diffusion-weighted images.

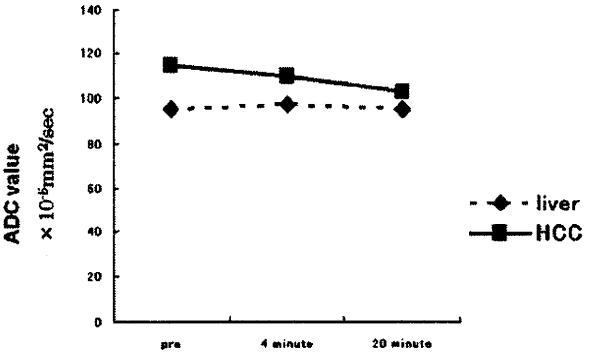

Figure 6. ADC values for the liver and HCC were not significantly different between pre- and postenhanced diffusion-weighted images.

ADC values of liver parenchyma were 95.5, 97.3, and 95.1 before and 4 and 20 min after injecting the contrast medium, and there was no significant difference between before and after contrast enhancement ($P > 0.05$). The ADC values of HCC were 114.7, 110.0, and 102.6 before and at 4 and 20 min after injecting the contrast medium, respectively, and no significant differences were found ($P > 0.05$) (Fig. 6).

Qualitative Analysis

There were no significant differences in the qualitative evaluation between the observers before and after contrast enhancement for both T2WI and DWI ($P > 0.05$) (Fig. 7). There were also no significant differences in the qualitative evaluation between the observers for each differentiated HCC on T2WI and DWI.

Interobserver variability is shown in Tables 1 and 2. There was fair or moderate agreement between observers 1 and 2 and observers 1 and 3 for T2WI. Moderate to almost perfect agreement was obtained between observers 2 and 3 for T2WI. Between observers 2 and 3, better agreement was obtained 4 and 20 min after injection than on plain T2WI. There was no change in the interobserver variability at any time period for DWI.

DISCUSSION

In the phantom study, signal intensity increased on T2WI at a concentration of contrast medium less than 0.2 mmol/L but decreased when the concentration exceeded 0.4 mmol/L. The contrast medium recirculated and accumulated into hepatocytes; therefore, its concentration in liver parenchyma was higher at 20 min after injecting the contrast medium compared with that after 4 min. The reason for increased liver parenchyma signal intensity at 4 min after injecting the contrast medium on T2WI was that the concentration in liver parenchyma was lower at 4 min than at 20 min after injection. Considering the extremely low accumulation in liver tumors (14), the liver tumor concentration was assumed to be less than 0.05 mmol/L, which was the minimum concentration for phantom study. Therefore, it is likely that the contrast

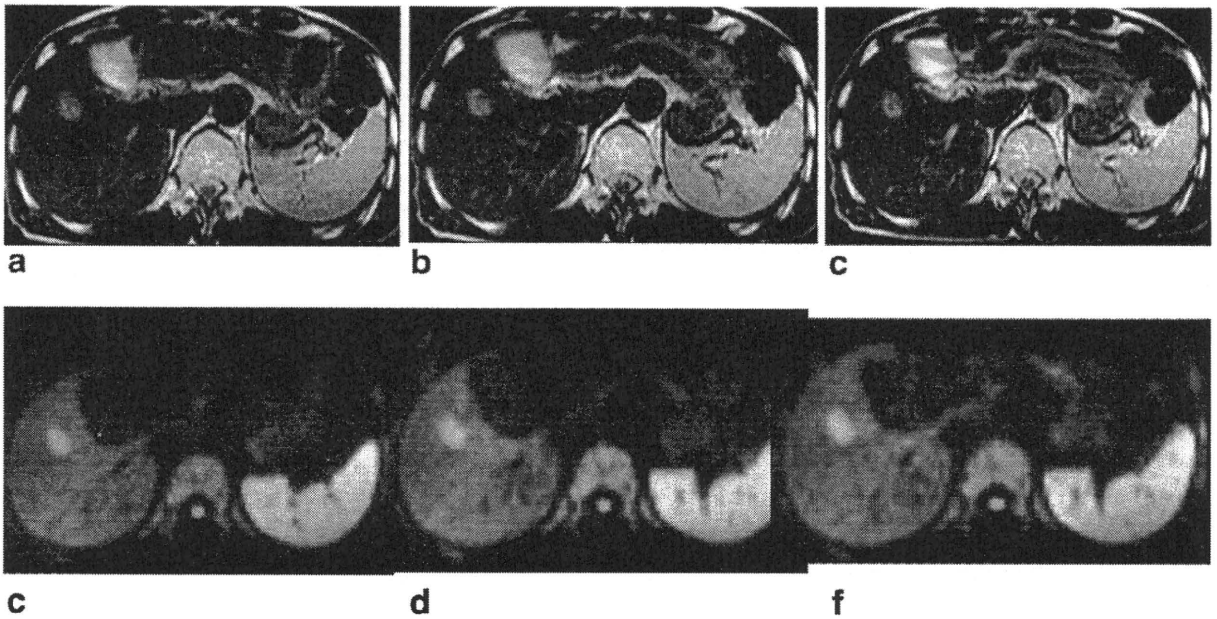

Figure 7. A 79-year-old man with HCC. The difference in conspicuity between pre- and postenhanced images was not that significant. **a**: Pre-enhanced T2-weighted image. **b**: Postenhanced T2-weighted image (after 4 min). **c**: Postenhanced T2-weighted image (after 20 min). **d**: Prediffusion-weighted image. **e**: Postenhanced diffusion-weighted image (after 4 min). **f**: Postenhanced diffusion-weighted image (after 20 min).

medium concentration increased only slightly, such that there was no significant difference in SNR of the tumor. This suggests that T2WI would show stable imaging features in liver parenchyma after an increase in the contrast medium concentration.

Brody et al reported the effect of Gd-EOB-DTPA on T2WI in liver parenchyma and found only a slight signal change (7). They reported about hemangiomas; the signal intensity of hemangiomas showed a tendency to increase, but there was no significant difference. In the present study, we reported about HCCs and found that there was no significant difference between before and after contrast enhancement. The visual assessment by all three observers also showed no significant difference; therefore, we thought that T2WI should be performed after injecting the contrast medium.

CNR of well-differentiated HCCs on T2WI tended to increase, but no significant difference was observed, indicating that the contrast medium accumulated in the tumor. Some well-differentiated HCCs show hypointensity on T2WI (15). When contrast medium accumulates in the hypointense lesion, the lesion signal increases. Therefore, hypointense lesions could have been obscured on T2WI. The present study included only one lesion type that showed hypointensity on T2WI, and hence further study is required.

Although the effect of Gd-DTPA on DWI has been reported, we could not find any report about the effect of Gd-EOB-DTPA on DWI (10). Gd-DTPA decreases the perfusion effect due to the intravascular contrast medium (16). The ADC value tended to decrease, but there was no statistically significant difference (10). In the present study, we did not find any statistically significant differences in ADC values using Gd-EOB-DTPA. Our phantom study also showed no significant changes in ADC values and the concentration of contrast medium had little effect. The changes in b = 800 signal intensity images were slight but that for b = 100 were great, which indicates that the influence of T2 relaxation was strong. This result shows that DWI can be performed soon after injecting the contrast medium.

It is necessary to differentially diagnose hemangiomas, hyperplastic lesions, and HCC in patients with chronic liver damage and cirrhosis. Because there is only a slight effect of contrast medium on hemangiomas (7), differential diagnosis of a hemangioma from HCC should not be difficult; however, further studies are required for hyperplastic lesions.

Table 1
Interobserver Agreement Among Three Observers (Kappa Values) for T2-Weighted Images

	Plain	After 4 min	After 20 min
Observer 1 vs 2	0.40	0.36	0.41
Observer 2 vs 3	0.59	0.87	0.73
Observer 3 vs 1	0.48	0.33	0.48

Table 2
Interobserver Agreement Among Three Observers (Kappa Values) for Diffusion-Weighted Images

	Plain	After 4 min	After 20 min
Observer 1 vs 2	0.52	0.48	0.41
Observer 2 vs 3	0.69	0.65	0.70
Observer 3 vs 1	0.37	0.30	0.24

There are several limitations to the present study. First, T2WI without fat suppression was used, which may have influenced CNR in the fatty liver cases. However, because only 2 patients had a fatty liver in the present study, we think the influence was small. Second, we did not consider the degree of liver damage and fibrosis. Severe liver damage and fibrosis may cause poor liver parenchymal enhancement and delayed optimal liver parenchymal enhancement (17). Therefore, these factors have the potential to influence T2WI and DWI intensity after enhancement. Finally, there were few histologically confirmed and small-sized lesions (<10 mm).

In conclusion, there were no significant differences in CNR and SNR of HCC before and after dynamic Gd-EOB-DTPA administration or during the hepatobiliary phase compared with background liver, which has a lower signal intensity during hepatobiliary phase imaging.

REFERENCES

1. Huppertz A, Haraida S, Kraus A, et al. Enhancement of focal liver lesions at gadoxetic acid-enhanced MR imaging: correlation with histopathologic findings and spiral CT – initial observations. Radiology 2005;234:468–478.
2. Vogl TJ, Kummel S, Hammerstingl R, et al. Liver tumors: comparison of MR imaging with Gd-EOB-DTPA and Gd-DTPA. Radiology 1996;200:59–67.
3. Schuhmann-Giampieri G, Schmitt-Willich H, Negishi WPC, Weinmann HJ, Speck U. Preclinical evaluation of Gd-EOB-DTPA as a contrast agent in MR imaging of the hepatobiliary system. Radiology 1992;183:59–64.
4. Hamm B, Staks T, Mühler A, et al. Phase I clinical evaluation of Gd-EOB-DTPA as a hepatobiliary MR contrast agent: pharmacokinetics, and MR imaging. Radiology 1995;195:785–792.
5. Zech CJ, Herrmann KA, Reiser MF, Schoenberg SO. MR imaging in patients with suspected liver metastases: value of liver-specific contrast agent Gd-EOB-DTPA. Magn Reson Med Sci 2007;6: 43–52.
6. Jeong YY, Mitchell DG, Holland GA. Liver lesion conspicuity: T2-weighted breath-hold fast spin-echo MR imaging before and after gadolinium enhancement – initial experience. Radiology 2001; 219:455–460.
7. Chang SD, Thoeni RF. Effect of T1 shortening on T2-weighted MRI sequences: comparison of hepatic mass conspicuity on images acquired before and after gadolinium enhancement. AJR Am J Roentgenol 2008;190:1318–1323.
8. Brody JM, Schafer L, Tung GA, Breuer J, Shamsi K. Conspicuity of liver hemangiomas: short tau inversion recovery, T1, and T2 imaging with gadolinium ethoxybenzyl diethylenetriaminepentaacetic acid. J Magn Reson Imging 2005;21:391–397.
9. Xu PJ, Yan FH, Wang JH, Lin J, Ji Y. Added value of breathhold diffusion-weighted MRI in detection of small hepatocellular carcinoma lesions compared with dynamic contrast-enhanced MRI alone using receiver operating characteristic curve analysis. J Magn Reson Imging 2009;29:341–349.
10. Kamel IR, Liapi E, Reyes DK, Zahurak M, Bluemke DA, Geschwind JFH. Unresectable hepatocellular carcinoma: serial early vascular and cellular changes after transarterial chemoembolization as detected with MR imaging. Radiology 2009;250:466–473.
11. Chiu FY, Jao JC, Chen CY, et al. Effect of intravenous gadolinium-DTPA on diffusion-weighted magnetic resonance images for evaluation of focal hepatic lesions. J Comput Assist Tomogr 2005;29:176–180.
12. Bruix J, Sherman M. Management of Hepatocellular carcinoma. Hepatology 2005;42:1208–1236.
13. Tajima T, Honda H, Taguchi K, et al. Sequential hemodynamic change in hepatocellular carcinoma and dysplastic nodules: CT angiography and pathologic correlation. AJR Am J Roentgenol 2002;178:885–897.
14. Reimer P, Rummeny EJ, Shamsi K, et al. Phase 2 clinical evaluation of Gd-EOB-DTPA: dose, safety aspects, and pulse sequence. Radiology 1996;199:177–183.
15. Earls JP, Theise ND, Weinreb JC, et al. Dysplastic nodules and hepatocellular carcinoma: thin-section MR imaging of explanted cirrhotic liver with pathologic correlation. Radiology 1996;201: 207–214.
16. Yamada K, Kubota H, Kizu O, et al. Effect of intravenous gadolinium-DTPA on diffusion-weighted images: evaluation of normal brain and infarcts. Stroke 2002;33:1799–1802.
17. Kim T, Murakami T, Hasuike Y, et al. Experimental hepatic dysfunction: evaluation by MRI with Gd-EOB-DTPA. J Magn Reson Imging 1997;7:683–688.

ELSEVIER

Clinical Imaging 34 (2010) 211–221

CLINICAL IMAGING

Real-time contrast-enhanced ultrasound imaging of focal liver lesions in fatty liver

Guang-Jian Liu[a], Wei Wang[a], Xiao-Yan Xie[a], Hui-Xiong Xu[a], Zuo-Feng Xu[a], Yan-Ling Zheng[a], Jin-Yu Liang[a], Fuminori Moriyasu[b], Ming-De Lu[c,*]

[a]*Department of Medical Ultrasonics, Institute of Diagnostic and Interventional Ultrasound, The First Affiliated Hospital of Sun Yat-Sen University, Guangzhou, China*

[b]*Department of Gastroenterology and Hepatology, Tokyo Medical University, Tokyo, Japan*

[c]*Department of Hepatobiliary Surgery, The First Affiliated Hospital of Sun Yat-Sen University, Guangzhou, China*

Received 20 March 2009; accepted 10 May 2009

Abstract

Purpose: The objective of this study was to investigate the contrast-enhanced ultrasound (CEUS) imaging features of focal liver lesions (FLLs) in fatty liver. **Method:** One hundred FLLs in 98 patients with fatty liver were evaluated with real-time CEUS. **Results:** All malignant FLLs showed hyperenhancement in arterial phase and contrast washout in portal and late phases. Among the FLLs, 3.3% of hemangiomas, 12.5% of focal nodular hyperplasias (FNHs), and 2.5% of focal fatty sparing lesions showed contrast washout in the late phase. The sensitivity and specificity for the characterization of hepatocellular carcinoma, metastasis, hemangioma, FNH, and focal fatty sparing lesions were 100% and 95.6%, 60% and 100%, 93.3% and 98.6%, 87.5% and 97.8%, and 92.6% and 100%, respectively. **Conclusions:** Correct characterization of FLLs in fatty liver by CEUS is possible based on their typical enhancement patterns.

Keywords: Fatty liver; Focal liver lesions; Contrast media; Ultrasound

1. Introduction

Real-time contrast-enhanced ultrasound (CEUS) using second-generation ultrasound contrast agents (UCAs) has been widely used as a noninvasive modality for the detection and characterization of focal liver lesions (FLLs) in clinical practice. The enhancement patterns of different kinds of FLLs on CEUS have been well described in normal liver parenchyma, and the CEUS diagnostic performance of FLLs in normal liver parenchyma has greatly improved compared with conventional gray-scale ultrasound, with 85–96% overall accuracy in differentiating malignant FLLs from benign ones and 81–88.5% overall accuracy in characterizing specific FLLs [1–5].

FLLs in diffuse liver disease such as liver cirrhosis or steatosis are very common in clinical practice. The presence of diffuse liver disease usually makes the appearance of FLLs on baseline gray-scale ultrasound unspecific and greatly increases the difficulty of characterization [6,7]. The CEUS imaging findings and diagnostic performance of FLLs in diffuse liver disease have been rarely reported in large scale at the present time [8–11].

This case series report describes our experience using real-time CEUS with a sulfur hexafluoride (SF6)-filled microbubble UCA in evaluating patients with a variety of FLLs in fatty liver.

2. Materials and methods

2.1. Patients

We retrospectively reviewed the results of conventional and CEUS examinations of 98 patients with FLLs and fatty

* Corresponding author. Department of Hepatobiliary Surgery, The First Affiliated Hospital of Sun Yat-Sen University, 58 Zhongshan Road 2, Guangzhou 510080, People's Republic of China. Tel.: +86 20 87765183; fax: +86 20 87765183.

E-mail address: lumd@21cn.com (M.-D. Lu).

0899-7071/09/$ – see front matter
doi:10.1016/j.clinimag.2009.07.003

liver who were admitted to our hospital between March 2004 and October 2006. The inclusion criteria were as follows: (a) fatty liver background confirmed by typical imaging findings; (b) number of FLLs less than 5; (c) no previously treated lesion; (d) no simple cystic lesion; and (e) diagnosis of FLLs confirmed by histopathology or clinical criteria. There were 59 men and 39 women aged 47.9±13.0 (mean±S.D.) years (range, 20–76 years).

Among these 98 patients, 82 had solitary lesions, 11 had two lesions, and 5 had multiple lesions. Only the most identifiable lesion on baseline gray-scale ultrasound was selected for evaluation with CEUS when a patient had two or multiple lesions. One hepatocellular carcinoma (HCC) patient suffered from twice-distant recurrence after radiofrequency ablation with at least 1-month interval. Thus, a total of 100 FLLs were evaluated in this study. The maximal diameter of the lesions ranged from 1.0 to 11.6 cm (mean, 3.1±1.9 cm), and the depth from the bottom of the lesion to the abdominal wall ranged from 3.5 to 15.0 cm (mean, 6.4±2.3 cm). The final diagnoses were malignant in 17 FLLs and benign in 83 FLLs, including 10 HCCs, 5 metastatic liver cancers (MLCs), 2 intrahepatic cholangiocarcinomas (ICCs), 30 hemangiomas, 8 focal nodular hyperplasias (FNHs), 42 focal fatty sparing lesions, 2 liver abscesses, and 1 solitary necrotic nodule (SNN) (Table 1).

The diagnoses of HCC were all confirmed by histopathology, with the specimens obtained by ultrasound-guided percutaneous biopsy (n=8) or surgery (n=2). Three of the MLC lesions were confirmed by histopathological examination, with the specimens obtained by percutaneous biopsy, and the remaining two lesions were confirmed by clinical data such as history of the primary malignancy, newly detected and continuously enlarged FLLs, and typical imaging findings on contrast-enhanced CT (CECT) or contrast-enhanced MRI [2,3,5]. The metastases were secondary to colorectal carcinoma in two patients, pancreatic carcinoma in two patients, and breast carcinoma in one patient. Both ICCs were confirmed histologically after surgical resection. All hemangiomas and focal fatty sparing lesions were proved by typical findings on CECT or contrast-enhanced MRI and lack of change in lesion size for at least 6 months on imaging follow-up [2,5]. All FNHs, liver abscesses, and SNNs were confirmed by ultrasound-guided percutaneous biopsy or aspiration and imaging follow-up for at least 6 months.

Fatty liver was confirmed by multiple imaging findings, with diagnostic criteria as follows: (a) on ultrasound: bright hepatic parenchyma with echogenicity higher than that of the right renal cortex and poor visualization or nonvisualization of portal vein borders, the diaphragm, or the posterior portion of the right lobe [12]; and (b) on CT: low attenuation of liver parenchyma on unenhanced CT, with values at least 10 HU lower than those of the spleen [13].

2.2. Contrast-enhanced sonography

CEUS examinations were performed with an Acuson Sequoia 512 scanner (Signature 7.2; Siemens Medical Solutions, Mountain View, CA) and a 4V1 vector transducer with frequencies of 1–4 MHz. The CEUS imaging technique and UCA used in the present study were contrast pulse sequencing (CPS) and SF6-filled microbubble contrast agent (SonoVue; Bracco, Milan, Italy), respectively.

Before administration of the UCA, baseline gray-scale ultrasound was performed to scan the entire liver. The imaging settings of the ultrasound scanner were optimized to get the best depiction of the target lesion. Diagnostic information, including the diameter, echogenicity, shape, and margin of each lesion, was recorded. After initiation of CPS imaging mode, a bolus injection of 2.4 ml of UCA was administered through a 20-gauge needle placed in the antecubital vein, followed by a 5-ml flush of 0.9% normal saline solution. Upon completion of the UCA injection, a timer is started simultaneously. The mechanical index (MI) indicated on the screen was between 0.14 and 0.21. The lesion was observed continuously for 6 min on CPS imaging mode. Based on previous literature, arterial phase is defined as 7–30 s after contrast agent injection, portal phase is defined as 31–120 s after contrast agent injection, and late phase is defined as 121–360 s after contrast agent injection [1–5]. The digital cine clips of baseline gray-scale ultrasound and the entire CEUS examination were stored in a hard disk incorporated in the scanner and converted from DICOM files into low compressed AVI files for subse-

Table 1
General features of FLLs (N=100)

Lesion	Lesion size (cm)	Depth (cm)	Number of lesions	Number of male/female patients	Patient age (years)
HCC	3.8±1.2[a] (1.6–5.3)	7.1±2.5[a] (4.4–10.9)	10	8/2	57.6±10.1[a] (41–73)
ICC	5.8, 7.8	6.8, 9.7	2	1/1	52, 60
MLC	3.0±0.6[a] (2.1–3.6)	8.3±1.8[a] (6.0–10.3)	5	2/3	58.0±9.7[a] (41–64)
Hemangioma	3.6±2.5[a] (1.0–11.6)	6.4±2.3[a] (3.5–15.0)	30	18/12	51.5±11.4[a] (34–75)
FNH	2.2±0.6[a] (1.6–2.9)	6.0±1.6[a] (4.0–8.1)	8	4/4	37.3±12.7[a] (24–64)
Focal fatty sparing lesions	2.3±0.9[a] (1.0–5.1)	5.8±1.8[a] (3.5–11.2)	42	25/17	43.1±11.3[a] (20–74)
Abscess	6.0, 9.2	5.5, 14.0	2	2/0	54, 76
SNN	1.7	5.5	1	1/0	28

[a] Data are expressed as mean size±S.D., with ranges indicated in parentheses.

quent analysis on a personal computer. In this study, no patient received additional administration of the contrast agent. All of the procedures were performed by one of two skilled investigators with at least 3 years' experience in using CEUS.

2.3. Image analysis

Baseline gray-scale ultrasound and CEUS images were displayed retrospectively from digital video files on a computer screen and evaluated in consensus by two investigators who were not involved in the ultrasound scanning and were unaware of the clinical and other imaging information of patients. The reviewers determined the diameters and echogenicity of the lesions on gray-scale ultrasound and evaluated the time of initial lesion enhancement, enhancement level, and pattern of each lesion at different phases of CEUS. The level of enhancement was divided into nonenhancing, hypoenhancing, isoenhancing, and hyperenhancing, according to the peak enhancement of lesion compared with the surrounding liver parenchyma. Contrast enhancement patterns were classified as homogenous, heterogeneous, rim, and peripheral nodular enhancement.

3. Results

3.1. HCC

On baseline gray-scale ultrasound, all HCCs were heterogeneously hypoechoic, with ovoid shape and sharp margins. After injection of the UCA, initial enhancement in all lesions appeared earlier than the initial enhancement of the liver parenchyma in the arterial phase of CEUS. There were eight (80%) lesions with homogeneous enhancement and two (20%) lesions with heterogeneous enhancement (Table 2). As to the enhancement level, all lesions exhibited hyperenhancement in the arterial phase. In the portal phase, all lesions demonstrated contrast enhancement washout and became hypoenhanced in eight (80%) patients and isoenhanced in two (20%) patients. In the late phase, all lesions were hypoenhancing compared with the surrounding liver parenchyma (Table 3).

When homogeneous or heterogeneous hyperenhancement in the arterial phase (with washout of contrast enhancement in the portal and late phases) was regarded as a positive finding of HCC, the sensitivity, specificity, positive predictive value (PPV), negative predictive value (NPV), and accuracy of real-time CEUS were found to be 100% (10 of 10), 95.6% (86 of 90), 71.4% (10 of 14), 100% (86 of 86), and 96% (96 of 100), respectively (Table 4).

3.2. MLC

MLCs were heterogeneously hyperechoic in two (40%) patients and hypoechoic in three (60%) patients on baseline gray-scale ultrasound. All lesions were ovoid in shape, with sharp margins. In the arterial phase of CEUS, all lesions enhanced earlier than the liver parenchyma. There were two (40%) lesions with homogeneous enhancement and three (60%) lesions with rim enhancement. As to the enhancement level, all lesions exhibited hyperenhancement in the arterial phase and hypoenhancement in the portal and late phases in relation to the surrounding liver parenchyma (Fig. 1).

When rim hyperenhancement in the arterial phase (with washout of contrast enhancement in the portal and late phases) was regarded as a positive finding of MLC, the sensitivity, specificity, PPV, NPV, and accuracy of real-time CEUS were found to be 60% (3 of 5), 100% (95 of 95), 100% (3 of 3), 97.9% (95 of 97), and 98% (98 of 100), respectively.

3.3. ICC

On baseline gray-scale ultrasound, both ICCs appeared to be heterogeneously hypoechoic, with ovoid shape and sharp margins. On CEUS images, both lesions showed heterogeneous hyperenhancement in the arterial phase, with one earlier emergence and one simultaneous emergence of enhancement when compared with the adjacent liver parenchyma. Both lesions appeared to be hypoenhancing in the portal and late phases and were misdiagnosed as HCC in the present study (Fig. 2).

Table 2
Enhancement patterns of FLLs in the arterial phase (N=100)

Pattern	Homogeneous enhancement	Heterogeneous enhancement	Peripheral nodular enhancement	Rim-like enhancement	No enhancement
HCC	8 (80)	2 (20)	–	–	–
ICC	–	2 (100)	–	–	–
MLC	2 (40)	–	–	3 (60)	–
Hemangioma	1 (3.3)	1 (3.3)	28 (93.4)	–	–
FNH	8 (100)	–	–	–	–
Focal fatty sparing lesions	40 (95.2)	–	–	–	2 (4.8)
Abscess	–	–	–	2 (100)	–
SNN	–	–	–	–	1 (100)

Data are numbers of lesions; data in parentheses are percentages.